Conformational Analysis Using Infrared and Vibrational Circular Dichroism Spectroscopies: The Chiral Cyclic Sulfoxides 1-Thiochroman-4-one *S*-Oxide, 1-Thiaindan *S*-Oxide and 1-Thiochroman *S*-Oxide

F. J. Devlin and P. J. Stephens*

Department of Chemistry, University of Southern California, Los Angeles, California 90089-0482

P. Scafato, S. Superchi, and C. Rosini

Dipartimento di Chimica, Università della Basilicata, Via N. Sauro 85, 85100 Potenza, Italy

Received: May 16, 2002; In Final Form: August 28, 2002

We report the conformational analysis of three chiral cyclic sulfoxides, 1-thiochroman-4-one *S*-oxide (**1**), 1-thiaindan *S*-oxide (**2**), and 1-thiochroman *S*-oxide (**3**). Vibrational unpolarized absorption (IR) and vibrational circular dichroism (VCD) spectroscopies are employed, in combination with ab initio density functional theory (DFT). DFT calculations predict two, two, and three conformations with energies spanning <1 kcal/mol in **1**, **2**, and **3**, respectively. Harmonic IR and VCD spectra of the conformations of **1**−**3**, predicted using DFT, are a sensitive function of conformational structure, and conformationally averaged IR and VCD spectra are consequently more complex than the spectra of individual conformations. Predicted IR and VCD spectra are compared to experimental spectra of CCl_4 and CS_2 solutions of **1**−**3** in the mid-IR spectral region. Calculated and experimental spectra are in good agreement, permitting assignment of very nearly all experimental bands. The analysis unambiguously confirms the presence of the conformations of **1**−**3** predicted by DFT.

Introduction

Vibrational spectra are exquisitely sensitive to molecular structure. In particular, different conformations of flexible molecules can exhibit very different spectra. It follows that, in principle, the vibrational spectra of a flexible molecule permit the elucidation of its conformational structures: conformational analysis.

Developments in ab initio density functional theory (DFT) over the last decade have made possible efficient and accurate predictions of harmonic vibrational frequencies, together with the harmonic dipole strengths and rotational strengths which determine the harmonic intensities of fundamental transitions in vibrational unpolarized absorption (infrared, IR) and vibrational circular dichroism (VCD) spectra.[1] Analytical derivative methods using perturbation-dependent basis sets have been developed and implemented for the calculation of harmonic force fields (Hessians),[2] atomic polar tensors (APTs),[2] and atomic axial tensors (AATs),[3] whence harmonic frequencies, dipole strengths, and rotational strengths are obtained. In the case of AATs, gauge-invariant (including) atomic orbitals (GIAOs)[4] are used. At the same time, the sophistication and accuracy of functionals has increased; particularly important has been the development of "hybrid" density functionals.[5] Consequently, it is now practicable to utilize IR and, in the case of chiral molecules, VCD spectra to carry out conformational analysis. Recent examples of this approach to conformational analysis include studies of 3-methylcyclohexanone[6] and two bicyclic naphthalenones.[7]

The use of vibrational spectroscopy for conformational analysis is particularly powerful in the case of flexible molecules exhibiting multiple conformations within an energy range of 1 kcal/mol when all conformations are substantially populated at room temperature and where the barriers between conformations are sufficiently low that conformational interconversion is fast on the NMR time scale. In this paper, we report studies of three flexible molecules in this category, the chiral cyclic sulfoxides 1-thiochroman-4-one *S*-oxide [2,3-dihydro-4*H*-1-benzothio-pyran-4-one *S*-oxide] (**1**), 1-thiaindan *S*-oxide [2,3-dihydrobenzo[*b*]thiophene *S*-oxide] (**2**), and 1-thiochroman *S*-oxide [2,3-dihydro-4*H*-1-benzothio-pyran *S*-oxide] (**3**),

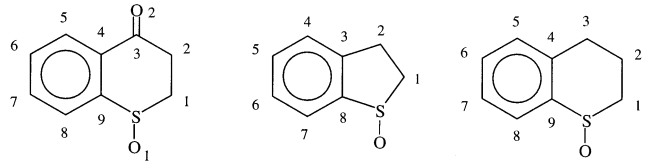

1 **2** **3**

using IR and VCD spectroscopies.

While the conformational analysis of flexible molecules is of intrinsic interest, it is also prerequisite to the understanding of other molecular properties. For example, conformational analysis is prerequisite to the prediction of the optical rotation (OR) and electronic circular dichroism (ECD) of flexible chiral molecules. DFT methods for predicting OR and ECD have recently been developed,[8] and we are currently studying their accuracy in the case of chiral sulfoxides. The conformational analyses of **1**−**3** reported here are foundational to our studies of the OR and ECD of **1**−**3**, to be published shortly.[9]

Methods

S-(+)- and *R*-(−)-sulfoxides **1**−**3** were synthesized from the corresponding sulfides, **4**−**6**, via asymmetric sulfoxidation.[10]

* To whom correspondence should be addressed. E-mail: pstephen@usc.edu or stephens_pj@hotmail.com.

10.1021/jp021225u CCC: $22.00
Published on Web 10/09/2002

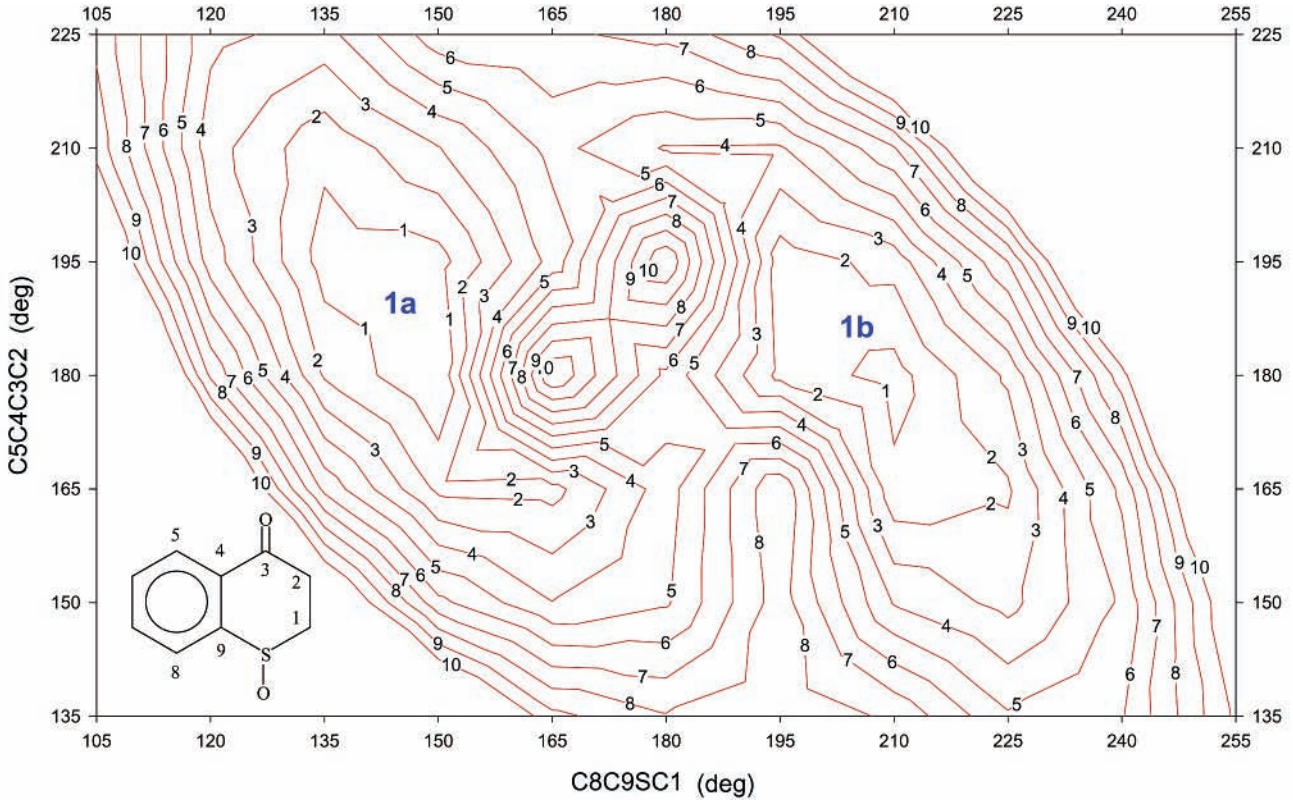

Figure 1. The B3LYP/6-31G* PES of S-**1**. The dihedral angles C5C4C3C2 and C8C9SC1 were varied in 15° steps. Contours are shown at 1 kcal/mol intervals.

Racemic sulfoxides **1**−**3** were obtained by H_2O_2 oxidation of the corresponding sulfides.[11] Detailed procedures are given in the Supporting Information. Enantiomeric excesses of (+) and (−) **1**−**3**, determined chromatographically, were as follows: (+)-**1**, 66%; (−)-**1**, 68%; (+)-**2**, 79%; (−)-**2**, 81%; (+)-**3**, 80%; (−)-**3**, 90%. The (+), (−), and (±) samples of **1**−**3** were of very similar chemical purities, as gauged by IR spectroscopy.

IR and VCD spectra of CCl_4 and CS_2 solutions of **1**−**3** have been obtained using Nicolet MX-1 and Bomem/BioTools Chiral*IR* spectrometers, respectively. IR and VCD spectra were measured at 1 and 4 cm^{-1} resolutions, respectively. VCD scans were 1 h. For each compound, VCD spectra of (+) and (−) enantiomers were both obtained, using the spectrum of the racemic mixture as the baseline. After conversion to $\Delta\epsilon$ units, VCD spectra were normalized to 100% enantiomeric excess (ee), giving the VCD spectra $\Delta\epsilon(+)$ and $\Delta\epsilon(-)$. "Half-difference" and "half-sum" spectra, $(^1/_2)[\Delta\epsilon(+) - \Delta\epsilon(-)]$ and $(^1/_2)[\Delta\epsilon(+) + \Delta\epsilon(-)]$, were then calculated. The former is the VCD of the (+) enantiomer. The latter is nonzero due to noise and artifacts and therefore provides a gauge of the reliability of the VCD spectrum. IR and VCD spectra were measured using KBr cells (Harrick) of path lengths 109, 239, and 597 μ. Experimental frequencies, dipole strengths, and rotational strengths were extracted from experimental IR and VCD spectra via Lorentzian fitting.[12]

Ab initio DFT calculations have been carried out using the Gaussian 98 program.[13] The functionals B3LYP[14] and B3PW91[5] have been used, together with the basis sets 6-31G*[15] and TZ2P.[16] Potential energy surface (PES) scans locate stable conformations. Geometry optimizations give equilibrium geometries. Harmonic force field calculations give harmonic vibrational frequencies and normal coordinates. Atomic polar tensor (APT) and atomic axial tensor (AAT) calculations then lead to harmonic vibrational dipole and rotational strengths.[1,3] All calculations use analytical derivative methods together with perturbation-dependent basis sets. In the case of AATs, gauge-invariant (including) atomic orbitals (GIAOs, also known as London orbitals) are used.[3] Rotational strengths are origin-independent. Harmonic IR and VCD spectra were derived from calculated harmonic frequencies, dipole strengths, and rotational strengths using Lorentzian band shapes.[12] The bandwidth parameter γ was set to 4.0 cm^{-1}, an arbitrary choice but representative of solution line widths.

Results

1-Thiochroman-4-one *S*-Oxide (1). The B3LYP/6-31G* PES of **1** has been scanned, varying simultaneously the two dihedral angles C5C4C3C2 and C8C9SC1 over the ranges 135°−225° and 105°−255°, respectively, i.e., −45° to +45° and −75° to +75° relative to the plane of the moiety C3C4C5C6C7C8C9S. The results are shown in Figure 1. Two well-defined minima in the PES are located. Energy minimization leads to two stable conformations, **1a** and **1b**, **1a** being lower in energy than **1b**. The values of key dihedral angles for the conformations **1a** and **1b** are given in Table 1. The energy difference between conformations **1a** and **1b** is given in Table 2. Further optimizations of the structures **1a** and **1b** have been carried out at the B3PW91/6-31G*, B3LYP/TZ2P, and B3PW91/TZ2P levels. Dihedral angles and energy differences for these structures are also given in Tables 1 and 2. The structures of **1a** and **1b** are insensitive to the choice of functional and basis set; key dihedral angles vary by <3°. The energy difference, $\Delta E_{ba} = E_{\mathbf{1b}} - E_{\mathbf{1a}}$, varies somewhat with functional and basis set, ranging from +0.42 to +0.82 kcal/mol.

The predicted structures of **1a** and **1b** are illustrated in Figure 2, where the B3LYP/TZ2P structures are shown. In both **1a** and **1b**, the C3O2C4C5C6C7C8C9S moiety is essentially planar. C2 is not far from this plane; C5C4C3C2 is within 10° of planar.

TABLE 1: Dihedral Angles of Conformations 1a and 1b[a]

	1a				1b			
	6-31G*		TZ2P		6-31G*		TZ2P	
	B3LYP	B3PW91	B3LYP[b]	B3PW91	B3LYP	B3PW91	B3LYP[c]	B3PW91
SC1C2C3	−64.8	−65.3	−63.9 (−62.6)	−64.7	67.6	68.1	66.4 (62.6)	67.2
C1C2C3C4	27.1	27.0	25.6 (38.2)	25.7	−33.4	−33.1	−33.5 (−38.2)	−33.5
C2C3C4C9	4.6	4.9	6.1 (−3.5)	6.3	−0.3	−0.7	0.0 (3.5)	−0.4
C3C4C9S	6.3	6.2	5.6 (−3.0)	5.5	−4.0	−3.8	−3.1 (3.0)	−2.9
C4C9SC1	−36.9	−37.4	−36.8 (−18.6)	−37.4	31.4	31.7	29.6 (18.6)	−30.1
C9SC1C2	62.5	63.2	62.4 (49.2)	63.2	−60.0	−60.7	−58.2 (−49.2)	−59.1
C5C4C3C2	−173.3	−172.9	−171.8 (174.1)	−171.6	178.5	178.2	179.7 (−174.1)	179.3
C5C4C3O2	6.7	7.0	8.2 (−3.7)	8.4	−2.0	−2.3	−1.1 (3.7)	−1.4
C8C9SC1	146.1	145.6	145.9 (162.1)	145.3	−151.8	−151.4	−153.2 (−162.1)	−152.7
C8C9SO1	33.1	32.4	33.9	33.0	99.5	99.8	98.1	98.5

[a] Dihedral angles in deg for the conformations of S-**1**. See text for atom numbering. [b] Dihedrals in parentheses are for structure **4a**. [c] Dihedrals in parentheses are for structure **4b**.

TABLE 2: Energies and Populations of the Conformations of 1, 2, and 3[a]

	B3LYP/6-31G*		B3PW91/6-31G*		B3LYP/TZ2P		B3PW91/TZ2P	
	E	*P*	*E*	*P*	*E*	*P*	*E*	*P*
1a	0.0	75.1	0.0	80.5	0.0	67.2	0.0	72.3
1b	0.64	24.9	0.82	19.5	0.42	32.8	0.56	27.7
2a	0.0	59.3	0.0	60.2	0.33	36.2	0.29	37.6
2b	0.22	40.7	0.24	39.8	0.0	63.8	0.0	62.4
3a[b]	0.0	37.9 (39.2)	0.16	30.2 (31.2)	0.0	54.1 (56.5)	0.0	49.0 (51.1)
3b[b]	0.07	33.5 (34.8)	0.0	39.8 (41.1)	0.50	22.9 (24.0)	0.35	26.8 (28.0)
3c[b]	0.24	25.0 (26.0)	0.23	26.8 (27.7)	0.62	18.7 (19.5)	0.52	20.1 (20.9)
3d	1.37	3.6	1.47	3.2	1.47	4.3	1.44	4.1

[a] Energies (*E*) in kcal/mol; populations (*P*) in percent. Populations are calculated from energies assuming Boltzmann statistics and $T = 293$ K. [b] Populations in parentheses are calculated ignoring conformation **3d**.

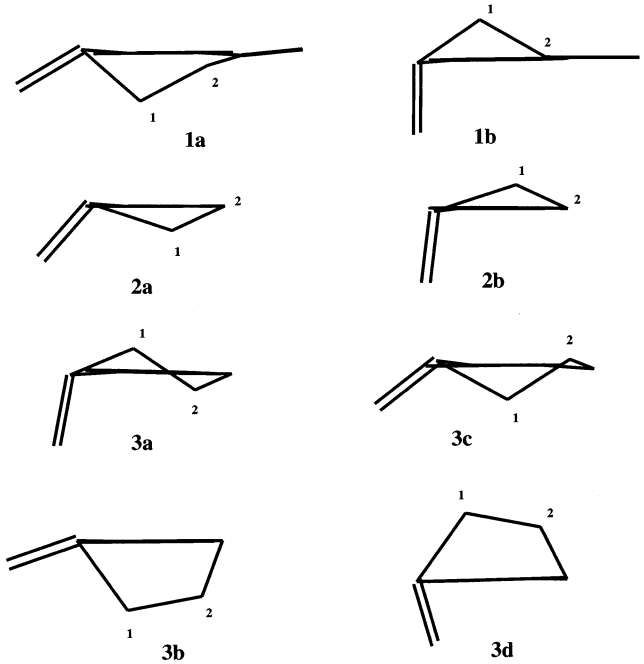

Figure 2. B3LYP/TZ2P structures of conformations **a** and **b** of S-**1**, conformations **a** and **b** of S-**2**, and conformations **a**, **b**, **c**, and **d** of S-**3**. H atoms are not included. The phenyl ring is at the rear as viewed.

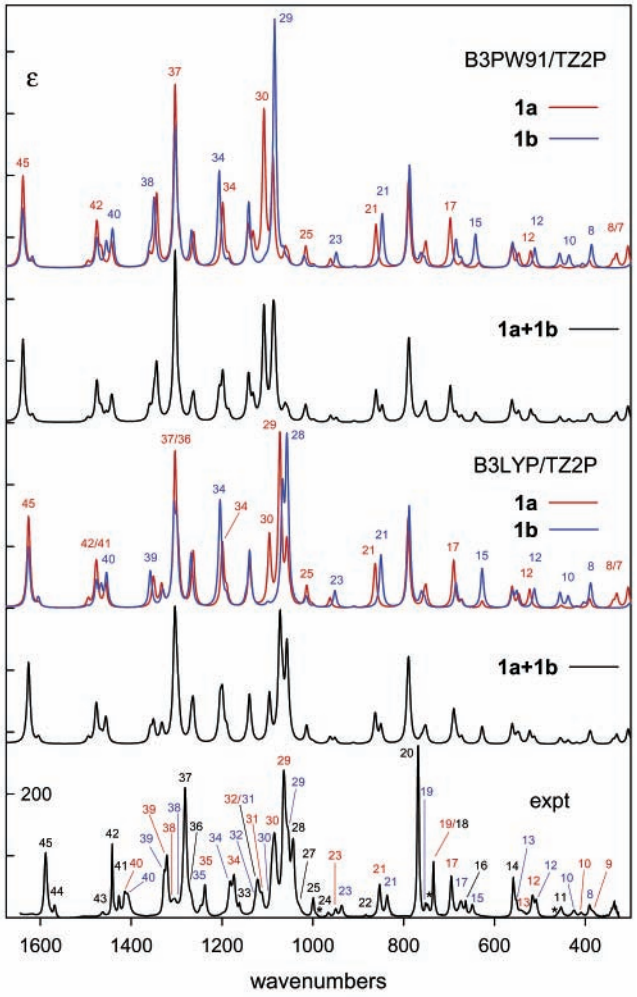

Figure 3. Calculated and experimental IR spectra of **1**. Spectra of the conformational mixture of **1a** and **1b** are obtained using populations of **1a** and **1b** from Table 2. The experimental spectrum is from Figure 5. In the assignment of the experimental spectrum, red and blue numbers indicate fundamentals of **1a** and **1b**, respectively; black numbers indicate fundamentals of **1a** and **1b** combined. Asterisks indicate bands not assigned to fundamentals of **1**.

The most prominent structural differences between conformations **1a** and **1b** involve the positions of C1 and O1. In **1a** and **1b**, C1 lies on opposite sides of the C3O2C4C5C6C7C8C9S plane. As a result, the orientation of the SO group relative to this plane is substantially different. In **1a**, O1 and C1 are on the same side of the plane; in **1b**, they are on opposite sides. In **1a**, the C8C9SO1 angle lies in the range 32°−34°; in **1b**, it is in the range 98°−100°.

Harmonic vibrational frequencies, dipole strengths, and rotational strengths for conformations **1a** and **1b**, calculated at the B3LYP/TZ2P and B3PW91/TZ2P levels, are given in Table 3. IR and VCD spectra calculated thence using Lorentzian band shapes are shown in Figures 3 and 4, together with conforma-

TABLE 3: Calculated and Experimental Frequencies, Dipole Strengths, and Rotational Strengths for 1[a]

				calculation[c]											
				B3LYP						B3PW91					
	experiment[b]			**a**			**b**			**a**			**b**		
mode	ν	D	R	ν	D	R	ν	D	R	ν	D	R	ν	D	R
46ab				1744	515.2	4.3	1747	462.8	−10.0	1764	513.8	5.2	1767	460.2	−9.1
45ab	1588	67.2		1626	105.0	−1.7	1626	69.9	3.9	1638	104.7	−2.5	1638	67.9	4.2
44ab	1569	10.1		1603	4.7	3.3	1604	11.1	−2.6	1617	5.1	3.5	1617	11.0	−3.0
43ab	1463	6.3		1495	10.1	1.5	1498	1.8	−2.7	1495	6.3	2.6	1499	0.9	−1.6
42ab	1442	36.3	−6.8	1477	42.0	−29.1	1477	31.6	7.0	1476	56.8	−18.6	1475	36.6	5.6
41ab	1427	17.3	11.1	1475	20.2	30.2	1466	23.4	−3.1	1466	19.0	18.4	1455	29.7	−1.6
40a	1414	22.1	−4.6	1456	31.5	−5.0				1443	33.0	−5.1			
40b	1407	28.7					1454	42.3	10.0				1441	47.8	10.7
39b	1327	33.4	−38.3				1358	49.8	−66.4				1359	20.7	−40.4
39a	1321	65.5	44.4	1351	41.1	46.3				1360	15.2	8.7			
38a	1308	10.2		1333	28.5	−4.8				1344	100.8	49.1			
38b	1303	10.5					1331	20.9	−0.8				1349	94.0	−45.3
37ab	1281	199.8	−25.5	1303	212.5	−95.8	1306	122.7	94.8	1303	260.0	−87.7	1303	196.2	103.7
36ab	1268	12.9	−10.2	1296	50.1	36.3	1299	93.9	−45.1	1291	11.5	16.2	1295	31.6	−45.3
35b	1246	9.6					1268	77.4	2.1				1267	51.6	4.7
35a	1238	33.0		1264	82.0	−1.5				1263	50.1	−4.0			
34b	1182	44.2	13.8				1204	165.9	31.1				1206	149.1	32.0
34a	1174	56.1	−26.6	1199	98.6	−31.8				1198	99.4	−35.1			
33ab	1162	9.7	−4.9	1189	22.1	−4.7	1190	12.7	−1.8	1185	14.2	−3.1	1186	8.4	−2.6
32b	1126	13.7					1147	8.9	−12.5				1142	25.0	−0.3
32a / 31b	1121	47.2	11.7	1140	72.9	0.8	1139	91.5	19.7	1142	63.0	−1.7	1141	83.4	12.3
31a	1113	25.3	−67.2	1134	6.0	−31.5				1131	44.1	−85.7			
30b	1094	4.3					1100	5.1	−6.6				1106	5.3	−5.8
30a	1086	182.5	92.2	1096	118.9	42.9				1108	260.8	117.7			
29a	1064	249.5	29.2	1073	299.9	28.9				1088	180.9	12.3			
29b	1055	102.7	13.0				1067	185.2	54.3				1084	427.3	20.1
28ab	1044	133.4		1057	103.1	8.7	1057	280.6	−35.9	1061	27.3	5.0	1065	19.7	−1.8
27ab	1030	2.7		1050	11.4	−6.4	1050	5.5	−2.9	1055	16.6	−6.1	1056	6.6	3.1
26ab				1025	0.1	0.0	1027	0.6	0.1	1022	0.1	0.6	1025	1.1	−0.7
25ab	999	21.1	12.9	1014	39.2	15.1	1015	18.8	8.5	1016	39.3	15.4	1019	20.6	1.4
24ab	966	6.5	−2.2	1001	4.1	−4.9	997	3.0	2.3	999	4.6	−4.6	995	2.9	1.7
23a	949	12.1	−13.9	962	19.3	−13.5				961	17.1	−15.1			
23b	936	20.0	−9.3				951	33.7	−11.0				948	30.2	−7.1
22ab	883	2.3	10.6	911	2.3	0.9	909	3.0	3.8	909	2.5	1.4	907	3.3	4.0
21a	853	61.6	14.1	863	96.5	18.3				861	94.1	21.2			
21b	836	46.0	−19.8[d]				850	116.4	−36.7				847	118.9	−41.8
20ab	768[d]	252.0[d]		790	210.5	−13.7	788	241.8	13.1	789	204.8	−10.8	787	242.9	9.9
19b	751[d]	10.5[d]					761	31.8	8.5				762	27.6	9.3
19a / 18ab	734[d]	67.6[d]		755	16.5	−5.2				757	15.4	−7.9			
				751	49.4	−5.7	754	19.9	−3.8	751	59.6	−9.5	754	20.2	−2.5
17a	695	87.5		690	129.0	−48.5				697	133.6	−44.8			
17b	674	54.0					685	67.6	26.4				685	75.4	29.4
16ab	663	20.5		672	18.3	−8.1	673	15.9	−7.4	672	14.2	−5.5	674	20.6	−11.6
15b	648	35.5					627	117.3	1.8				642	97.8	7.1
15a				627	20.2	24.9				635	14.9	20.1			
14ab	558	80.3		561	69.8	−21.6	560	53.0	18.6	562	72.5	−19.0	561	74.9	0.9
13b	552	26.4					551	51.4	9.1				554	36.9	24.9
13a	540	34.8		546	43.4	29.4				547	46.0	24.2			
12a	516	64.1		522	66.1	41.8				520	60.4	46.8			
12b	508	43.5					512	69.8	−47.6				511	72.5	−49.1
11ab	453	45.8		453	11.7	−5.5	456	62.2	0.5	455	10.6	−2.8	456	58.6	1.5
10b	425	36.9					438	49.2	−25.6				436	52.9	−27.4
10a	409	18.0		419	9.0	−6.1				417	10.2	−8.5			
9b							404	20.1	4.4				407	15.5	4.3
8b	391	45.2					388	120.1	4.2				386	112.6	1.8
9a	382	31.2		391	45.0	−4.9				391	36.4	−3.6			
8a				339	29.5	−27.8				339	30.4	−24.8			
7ab				331	76.2	24.5	304	16.0	5.8	331	74.0	24.7	303	10.2	5.8
6ab				306	126.7	20.9	291	117.4	−56.2	306	132.4	19.9	290	121.7	−59.0

[a] Frequencies, ν, in cm^{-1}; dipole strengths, D, in 10^{-40} esu^2 cm^2; rotational strengths, R, in 10^{-44} esu^2 cm^2. Experimental rotational strengths are for (+)-**1**; calculated rotational strengths are for S-1. [b] From Lorentzian fitting of spectra in CCl_4, unless indicated. [c] TZ2P basis set. [d] From spectra in CS_2.

tionally averaged spectra obtained using percentage populations of **1a** and **1b** calculated from the DFT energy difference assuming Boltzmann statistics (Table 2).

IR and VCD spectra of CCl_4 and CS_2 solutions of **1** have been measured in the mid-IR spectral region. Spectra of **1** in CCl_4 and CS_2 solutions are very similar. Composite IR and VCD

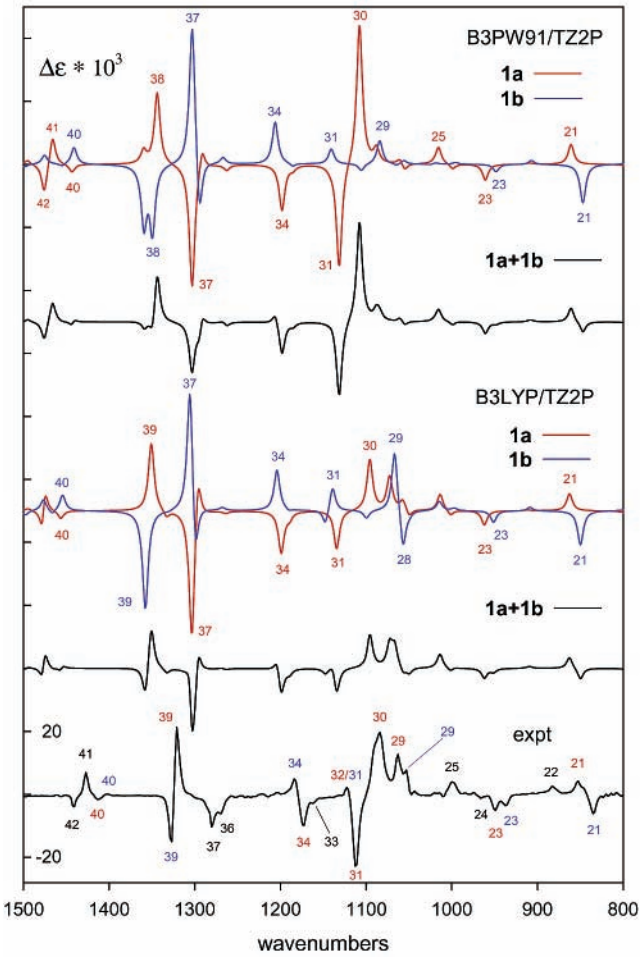

Figure 4. Calculated and experimental VCD spectra of **1**. Calculated spectra are for S-**1**. Spectra of the conformational mixture of **a** and **b** are obtained using populations of **1a** and **1b** from Table 2. The experimental spectrum is for (+)-**1** and is from Figure 5. In the assignment of the experimental spectrum, red and blue numbers indicate fundamentals of **1a** and **1b**, respectively; black numbers indicate fundamentals of **1a** and **1b** combined.

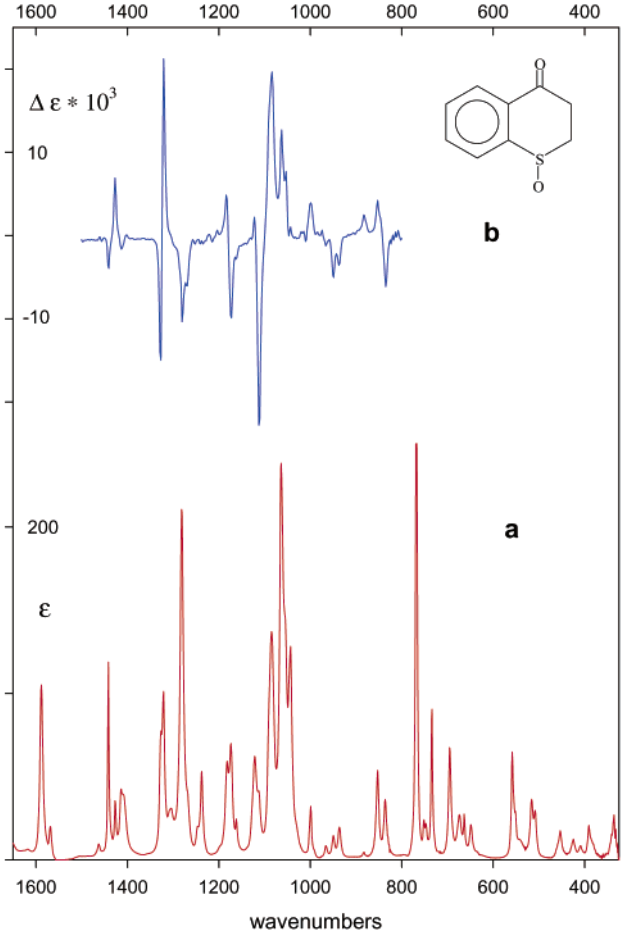

Figure 5. Experimental IR (a) and VCD (b) spectra of **1**: (a) 325−715 and 900−1650 cm^{-1}, 0.12 M in CCl_4, 597 μ path; 715−825 cm^{-1}, 0.05 M in CS_2, 597 μ path; 825−900 cm^{-1}, 0.12 M in CCl_4, 239 μ path; (b) 800−842 cm^{-1}, 0.05 M in CS_2, 597 μ path; 842−1050 and 1130−1500 cm^{-1}, 0.12 M in CCl_4, 597 μ path; 1050−1130 cm^{-1}, 0.12 M in CCl_4, 239 μ path. The IR spectrum is for (+)-**1**; the VCD spectrum is the "half-difference" spectrum, $(1/2)[\Delta\epsilon(+) - \Delta\epsilon(-)]$ (see text).

spectra are shown in Figure 5. The experimental IR spectrum of **1** is compared to the calculated IR spectra in Figure 3. Overall, the B3LYP/TZ2P and B3PW91/TZ2P spectra are both in good agreement with the experimental spectrum and permit convincing assignment of the majority of the bands observed experimentally. Our assignment is detailed in Table 3 and Figure 3. The analysis of the IR spectrum of **1** unambiguously demonstrates the presence of the two conformations, **1a** and **1b**, in CCl_4 and CS_2 solutions. Fundamentals 10, 12, 17, 21, 23, 29−31, 34, 35, 39, and 40 of **1a** and fundamentals 8, 10, 12, 13, 15, 17, 21, 23, 29, 34, 35, 39, and 40 of **1b** are clearly resolved and unambiguously assignable.

The reliability of our assignment can be further defined by quantitative comparison of calculated and experimental vibrational frequencies and dipole strengths. Experimental parameters obtained via Lorentzian fitting of the IR spectrum are given in Table 3. Calculated and experimental parameters are compared in Figures 6 and 7. Calculated dipole strengths are conformationally averaged. With few exceptions, calculated frequencies exceed experimental frequencies, the percentage differences lying in the range 0−4%, as is typically the case for B3LYP/TZ2P and B3PW91/TZ2P harmonic frequencies.[12,17] The agreement of calculated and experimental dipole strengths is also comparable to that found in previous studies.[12,17] Agreement is good for both functionals, with the exception of four modes, specifically, 28−30 of **1a** and 28 of **1b**.

The experimental VCD spectrum of (+)-**1** is compared to the calculated VCD spectra for S-**1** in Figure 4. VCD originating in fundamentals 21, 23, 29−31, 34, 39, and 40 of conformation **1a** and in fundamentals 21, 23, 29, 34, and 39 of conformation **1b** is clearly observed, further substantiating the presence of both **1a** and **1b**. In addition, VCD originating in the unresolved fundamentals 22, 24, 25, 33, 36, 37, 41, and 42 of **1a** and **1b** is observed. Experimental rotational strengths obtained via Lorentzian fitting of the VCD spectrum are given in Table 3. Calculated and experimental rotational strengths are compared in Figure 8. Calculated rotational strengths are conformationally averaged. The agreement is typical of that obtained in previous studies.[12,17] Agreement is good for both functionals, with the exception of two modes, 30 and 31 of **1a**.

While similar overall, B3LYP/TZ2P and B3PW91/TZ2P IR and VCD spectra do exhibit significant differences, most markedly for modes 27−32, indicating that the normal coordinates for these modes are sensitive to the choice of functional. In comparison to experiment, neither functional is definitively superior. The B3PW91 dipole strength for mode 30 of **1a** and the rotational strengths for modes 30 and 31 of **1a** are in substantially better agreement with experimental values (Table 3 and Figures 7 and 8). On the other hand, for modes 28 of **1a**

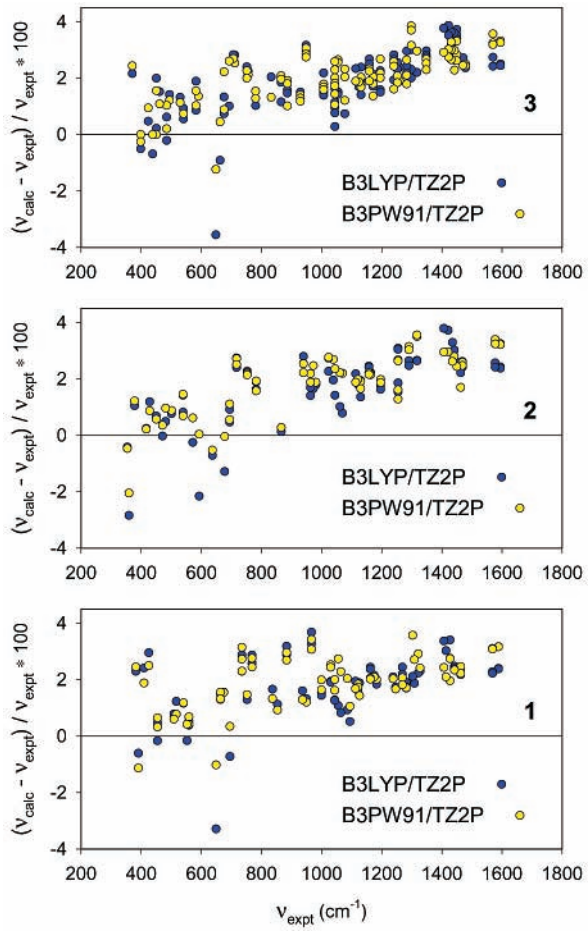

Figure 6. Comparison of calculated and experimental frequencies of **1**, **2**, and **3**.

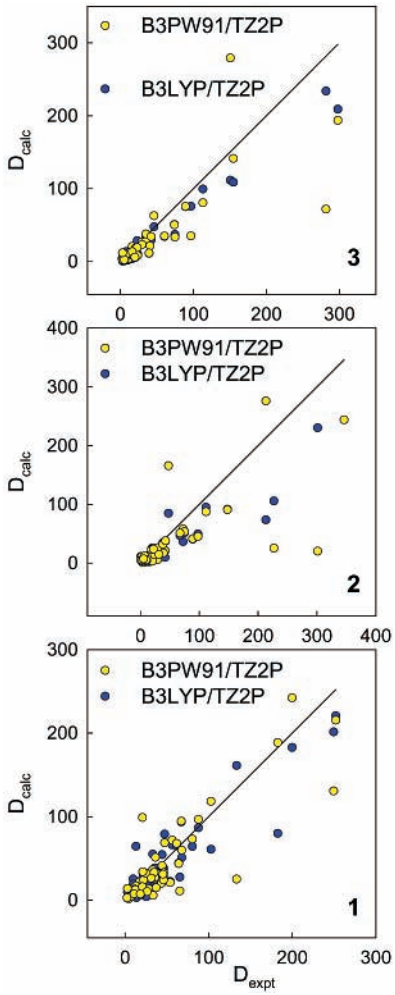

Figure 7. Comparison of calculated and experimental dipole strengths of **1**, **2**, and **3**. Calculated dipole strengths are population-weighted averages. The lines are of slope +1. Dipole strengths are in 10^{-40} esu^2 cm^2.

and **1b** and 29 of **1a**, it is the B3LYP dipole strengths which are in better agreement with experiment.

1-Thiaindan *S*-Oxide (2). The B3LYP/6-31G* PES of **2** has been scanned, varying the dihedral angle C7C8SC1 over the range 105°−255°, i.e., −75° to +75° relative to the plane of the moiety C2C3C4C5C6C7C8S. The results are shown in Figure 9. Two well-defined minima are located. Energy minimization at the B3LYP/6-31G*, B3PW91/6-31G*, B3LYP/TZ2P, and B3PW91/TZ2P levels leads to two stable conformations, **2a** and **2b**. Key dihedral angles for the structures of **2a** and **2b** are given in Table 4. The energy differences of conformations **2a** and **2b** are given in Table 2. The structures of **2a** and **2b** are insensitive to the choice of functional and basis set; key dihedral angles vary by <4°. The energy difference varies with functional and basis set. For both functionals, at the 6-31G* basis set level **2a** is predicted to be lower in energy than **2b**; at the TZ2P basis set level the energy ordering is reversed. The energy difference, $\Delta E_{ba} = E_{\mathbf{2b}} - E_{\mathbf{2a}}$, ranges from −0.33 to +0.24 kcal/mol.

The predicted structures of **2a** and **2b** are illustrated in Figure 2, in which the B3LYP/TZ2P structures are shown. In both **2a** and **2b**, the C2C3C4C5C6C7C8S moiety is essentially planar. In **2a** and **2b**, C1 lies on opposite sides of the C2C3C4C5C6C7C8S plane. As a result, the orientation of the SO group relative to this plane is substantially different. In **2a**, C1 and O are on the same side of the plane; in **2b**, they are on opposite sides. In **2a**, the C7C8SO angle lies in the range 51°−56°; in **2b**, it is 86°−87°.

Harmonic vibrational frequencies, dipole strengths, and rotational strengths for conformations **2a** and **2b**, calculated at the B3LYP/TZ2P and B3PW91/TZ2P levels, are given in Table 5. IR and VCD spectra calculated thence using Lorentzian band shapes are given in Figures 10 and 11, together with conformationally averaged spectra obtained using percentage populations of **2a** and **2b** calculated from the DFT energy difference assuming Boltzmann statistics (Table 2).

IR and VCD spectra of CCl_4 and CS_2 solutions of **2** have been measured in the mid-IR spectral region. Spectra of **2** in CCl_4 and CS_2 solutions are very similar. Composite IR and VCD spectra are shown in Figure 12. The experimental IR spectrum of **2** is compared to the calculated IR spectra in Figure 10. Overall, the B3LYP/TZ2P and B3PW91/TZ2P spectra are both in good agreement with the experimental spectrum and permit convincing assignment of the majority of the bands observed experimentally. Our assignment is detailed in Table 5 and Figure 10. The analysis of the IR spectrum of **2** unambiguously demonstrates the presence of the two conformations, **2a** and **2b**, in CCl_4 and CS_2 solutions. Fundamentals 6, 8, 9, 11, 12, 17, 21, 24, 25, and 35 of **2a** and fundamentals 7, 8, 9, 11, 12, 21, 24, 25, 26, 35, 36, and 37 of **2b** are clearly resolved and unambiguously assignable.

Lorentzian fitting of the experimental IR spectrum of **2** leads to the frequencies and dipole strengths given in Table 5. Calculated and experimental frequencies and dipole strengths are compared in Figures 6 and 7. Calculated dipole strengths are conformationally averaged. The agreement of calculated and

TABLE 4: Dihedral Angles of Conformations 2a and 2b[a]

	2a				2b			
	6-31G*		TZ2P		6-31G*		TZ2P	
	B3LYP	B3PW91	B3LYP[b]	B3PW91	B3LYP	B3PW91	B3LYP[c]	B3PW91
SC1C2C3	−33.9	−34.9	−31.7 (−31.4)	−32.8	33.1	33.9	32.0 (31.3)	32.7
C1C2C3C8	20.9	21.2	19.8 (22.7)	20.2	−20.4	−20.6	−19.6 (−22.6)	−19.8
C2C3C8S	2.4	2.7	1.8 (−2.5)	2.2	−2.0	−2.2	−2.3 (2.5)	−2.5
C3C8SC1	−19.5	−20.3	−17.9 (−14.4)	−18.8	18.6	19.2	18.3 (14.4)	18.9
C8SC1C2	30.5	31.5	28.3 (26.3)	29.5	−29.5	−30.4	−28.7 (−26.3)	−29.5
C4C3C2C1	−159.2	−158.8	−160.4 (−160.1)	−160.0	160.1	159.9	161.4 (160.2)	161.1
C7C8SC1	162.6	162.2	164.3 (166.3)	163.8	−164.8	−164.5	−165.3 (−166.3)	−164.9
C7C8SO	51.9	51.3	55.1	54.3	86.1	86.4	86.5	86.7

[a] Dihedral angles in deg for the conformations of S-**2**. See text for atom numbering. [b] Dihedrals in parentheses are for structure **5a**. [c] Dihedrals in parentheses are for structure **5b**.

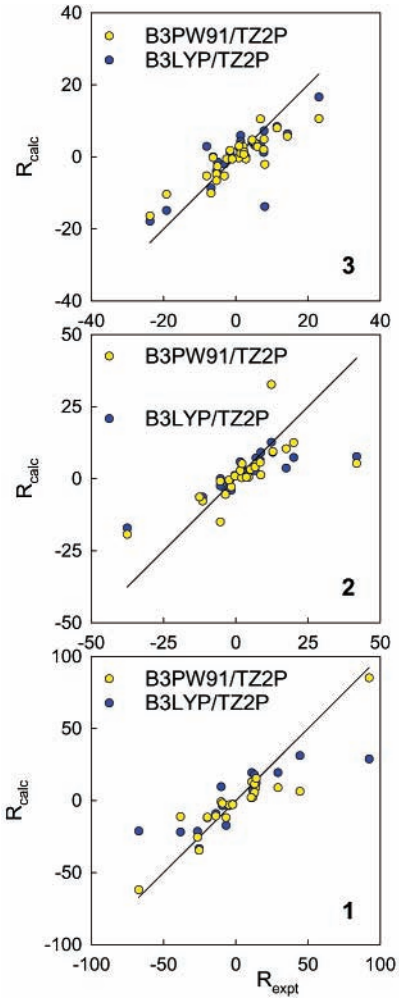

Figure 8. Comparison of calculated and experimental rotational strengths of **1**, **2**, and **3**. Calculated rotational strengths are for the *S* absolute configuration and are population-weighted averages; experimental rotational strengths are for the (+) isomer. The lines are of slope +1. Rotational strengths are in 10^{-44} esu^2 cm^2.

experimental frequencies and dipole strengths is comparable to that observed for **1**. In the case of the dipole strengths, agreement is good for both functionals, with the exception of four modes, specifically modes 24 and 25 of **2a** and **2b**.

The experimental VCD spectrum of (+)-**2** is compared to the calculated VCD spectra for S-**2** in Figure 11. VCD originating in fundamentals 17, 21, 25, and 26 of conformation **2a** and fundamentals 17, 21, 25, 26, 35, and 37 of conformation **2b** is clearly observed, further substantiating the presence of both **2a** and **2b**. In addition, VCD originating in the unresolved

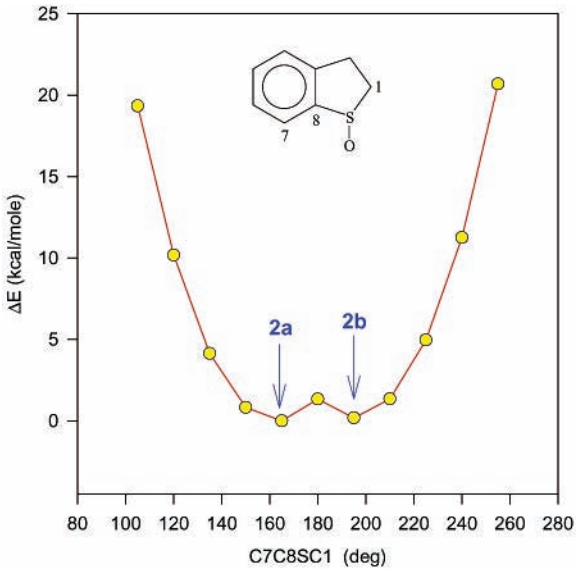

Figure 9. The B3LYP/6-31G* energy of S-**2** as a function of the dihedral angle C7C8SC1.

fundamentals 16, 19, 20, 24, 27−32, 34, and 38 is observed. Experimental rotational strengths obtained via Lorentzian fitting of the VCD spectrum are given in Table 5. Calculated and experimental rotational strengths are compared in Figure 8. Calculated rotational strengths are conformationally averaged. Agreement is comparable to that observed for **1** and is good for both functionals, with the exception of five modes, specifically modes 25, 26, and 27 of **2a** and 25 and 27 of **2b**.

The differences in B3LYP/TZ2P and B3PW91/TZ2P IR and VCD spectra are most marked for modes 23−27. B3LYP gives clearly superior agreement with experiment for the dipole strengths of modes 24 and 25 of **2a** and mode 24 of **2b** and for the rotational strengths of modes 25 and 26 of **2a** (Table 5 and Figures 7 and 8).

1-Thiochroman *S*-Oxide (3). The B3LYP/6-31G* PES of **3** has been scanned, varying simultaneously the two dihedral angles C5C4C3C2 and C8C9SC1 over the range 105°−255°, i.e., −75° to +75° relative to the plane of the moiety C3C4C5C6C7C8C9S. The results are shown in Figure 13. Four well-defined minima in the PES are located. Energy minimization at the B3LYP/6-31G*, B3PW91/6-31G*, B3LYP/TZ2P, and B3PW91/TZ2P levels leads to four stable conformations, **3a**−**3d**. Key dihedral angles for the structures of **3a**−**3d** are given in Table 6. The energy differences of conformations **3a**−**3d** are given in Table 2. The structures of **3a**−**3d** are insensitive to the choice of both functional and basis set; key dihedral angles vary by <4°. The energy differences vary with functional and basis set. The ordering is **3a** < **3b** < **3c** < **3d**, except at the

TABLE 5: Calculated and Experimental Frequencies, Dipole Strengths, and Rotational Strengths for 2[a]

				calculation[c]											
				B3LYP						B3PW91					
	experiment[b]			**a**			**b**			**a**			**b**		
mode	ν	D	R	ν	D	R	ν	D	R	ν	D	R	ν	D	R
40ab	1594	6.2		1633	2.3	−1.5	1632	5.2	−0.2	1646	2.5	−1.3	1646	5.8	−0.2
39ab	1577	3.2		1618	0.7	0.4	1615	3.3	−0.8	1631	0.8	0.4	1628	3.7	−0.8
38ab	1468	29.4	−11.5	1506	16.4	−0.8	1504	19.4	−9.6	1506	26.5	−3.7	1504	26.0	−10.3
37a	1463	4.6	−1.6	1495	28.1	−11.1				1487	28.9	−7.6			
37b	1450	29.1	7.0				1487	32.7	11.3				1485	20.7	8.0
36a	1441	3.0		1485	10.9	2.2				1482	3.9	0.3			
36b	1435	15.5					1482	3.8	2.1				1473	13.9	5.9
35a	1420	7.0		1473	14.8	1.8				1462	17.7	2.1			
35b	1406	20.1	5.0				1460	14.8	4.7				1448	17.9	5.1
34ab	1317	4.5	−2.4	1352	0.5	1.7	1352	1.5	−2.9	1364	0.8	0.6	1364	2.0	−1.1
33ab	1290	4.8	−0.4	1324	1.2	−1.4	1322	1.0	2.5	1331	1.2	−2.3	1329	0.7	2.9
32ab	1254	23.0	12.8	1292	10.1	−19.6	1293	11.0	25.6	1287	9.1	−17.9	1287	9.4	24.1
31ab			−3.6	1273	4.4	−0.3	1277	3.5	−6.5	1270	6.1	3.0	1274	4.4	−8.8
30ab	1196	15.6	4.4	1215	7.6	−6.8	1217	5.4	6.6	1218	11.0	−7.3	1220	6.1	5.2
29ab	1163	7.1	6.6	1188	6.3	−7.3	1189	4.7	8.5	1188	12.7	−11.2	1189	10.8	13.2
28ab	1157	5.4	2.0	1185	6.2	−4.4	1185	5.1	4.2	1182	3.6	−2.2	1183	2.2	1.7
27ab	1130	72.3	−37.6	1145	32.6	−14.0	1152	38.9	−18.8	1149	43.0	−10.7	1152	67.1	−24.5
26b	1120	14.7	20.0				1141	21.6	11.6				1143	18.7	20.0
26a	1113	2.1	−5.4	1137	9.1	−6.8				1134	29.6	−39.8			
25a	1069	47.4	12.3[e]	1077	234.5	34.9				1093	441.3	86.9			
25b	1061	213.1	41.8[e]				1072	115.4	12.0				1085	442.5	8.5
24b	1045	301.0	−5.4[e]				1059	360.9	−11.9				1069	32.7	−2.3
24a	1038	226.8		1059	292.1	20.9				1066	67.5	1.2			
23ab	1023	29.1		1047	6.1	0.6	1046	13.1	0.4	1051	6.1	0.6	1052	6.1	−0.4
22ab				1009	0.2	0.2	1010	0.3	0.1	1008	0.1	0.1	1008	0.2	0.1
21a	981	0.6	1.5	999	31.0	16.4				1000	12.2	7.5			
21b	972	20.2	8.6				988	40.6	14.2				996	5.1	2.1
20ab	963	41.7	17.4	976	4.7	1.7	979	12.5	4.9	984	10.3	6.7	981	27.4	12.6
19ab	940	3.0	2.1	966	4.8	2.4	964	5.5	5.6	964	4.6	2.9	961	4.8	6.5
18ab				888	1.9	2.1	887	0.4	0.6	887	1.9	2.1	886	0.3	0.3
17a	865	7.0	3.6	867	13.2	2.0				868	12.2	1.3			
17b	841[e]		8.4[e]				857	1.9	9.8				857	1.7	8.9
16ab	782[d]	74.7[d]	−12.6[e]	797	39.2	11.9	795	58.5	−16.8	797	38.1	12.3	794	62.7	−17.6
15ab	752[d]	345.9[d]		769	280.3	2.5	768	223.2	−0.6	768	283.7	0.7	768	219.7	−1.5
14ab	717[d]	67.1[d]		734	23.2	−2.6	737	59.9	−24.6	735	26.1	−4.1	736	65.9	−25.0
13ab	694	23.5		697	4.1	−1.3	700	17.6	1.8	698	4.5	−1.2	701	20.0	2.1
12a	677	7.2		668	28.7	16.4				677	32.2	19.8			
12b	636	10.4					632	3.6	5.8				633	6.7	2.5
11b	592	37.9					580	53.8	21.2				593	51.3	23.2
11a	571	9.8		570	17.0	−11.4				574	14.3	−11.6			
10ab	539	147.9		543	55.6	−13.7	546	112.0	−23.9	543	54.3	−13.0	547	112.9	−22.1
9b	500	39.1					504	27.3	1.0				505	27.8	0.6
8b	481	111.1					483	149.0	32.1				485	140.0	31.3
9a	470	18.7		470	65.4	−11.1				472	60.3	−9.9			
8a	450	42.5		453	102.4	35.8				452	100.8	36.8			
7b	428	88.6					433	63.6	−30.4				432	66.7	−30.3
7a	416	5.2		417	22.3	−11.7				417	19.2	−14.0			
6a	377	31.4		381	43.8	−0.3				382	39.4	0.0			
5a	359	22.0		349	62.1	7.6				352	62.9	7.4			
6b	353	97.5					352	78.0	2.3				352	72.5	2.0

[a] Frequencies, ν, in cm^{-1}; dipole strengths, D, in 10^{-40} esu^2 cm^2; rotational strengths, R, in 10^{-44} esu^2 cm^2. Experimental rotational strengths are for (+)-**2**; calculated rotational strengths are for S-**2**. [b] From Lorentzian fitting of IR spectra in CCl_4 solution, unless indicated. [c] TZ2P basis set. [d] CS_2 solution IR spectra. [e] CS_2 solution VCD spectra.

B3PW91/6-31G* level where the ordering of **3a** and **3b** is **3b** < **3a**. The span of energies of **3a**−**3d** ranges from 1.37 to 1.47 kcal/mol. Excluding **3d**, the span of energies of **3a**−**3c** ranges from 0.23 to 0.62 kcal/mol.

The predicted structures of **3a**−**3d** are illustrated in Figure 2, where the B3LYP/TZ2P structures are shown. In all conformations, the C3C4C5C6C7C8C9S moiety is essentially planar. In **3a** and **3c**, C1 and C2 are on opposite sides of this plane; in **3b** and **3d**, C1 and C2 are on the same side of this plane. The orientations of the SO group vary accordingly. In **3a** and **3d**, the O atom and C1 are on opposite sides of the C3C4C5C6C7C8C9S plane; in **3b** and **3c**, O and C1 are on the same side of this plane. In **3a**−**3d**, the C8C9SO angle lies in the ranges 89°−92°, 18°−20°, 39°−43°, and 118°−120° respectively.

Harmonic vibrational frequencies, dipole strengths, and rotational strengths for conformations **3a**−**3c**, calculated at the B3LYP/TZ2P and B3PW91/TZ2P levels, are given in Table 7. IR and VCD spectra calculated thence using Lorentzian band shapes are shown in Figures 14−16, together with conformationally averaged spectra obtained using percentage populations of **3a**−**3c** calculated from the DFT energy differ-

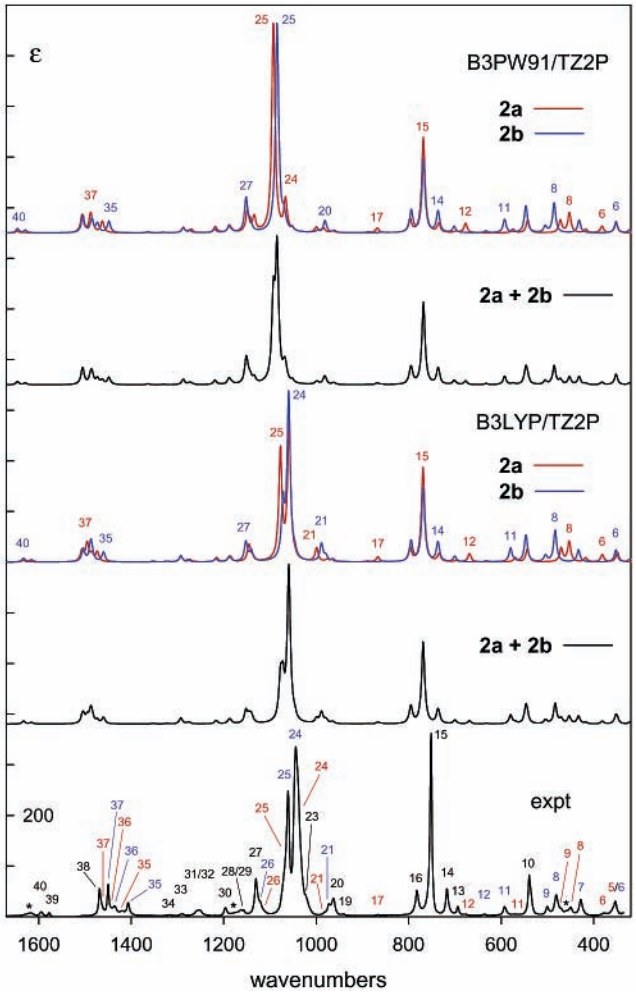

Figure 10. Calculated and experimental IR spectra of **2**. Spectra of the conformational mixture of **2a** and **2b** are obtained using populations of **2a** and **2b** from Table 2. The experimental spectrum is from Figure 12. In the assignment of the experimental spectrum, red and blue numbers indicate fundamentals of **2a** and **2b**, respectively, while black numbers indicate fundamentals of **2a** and **2b** combined. Asterisks indicate bands not assigned to fundamentals of **2**.

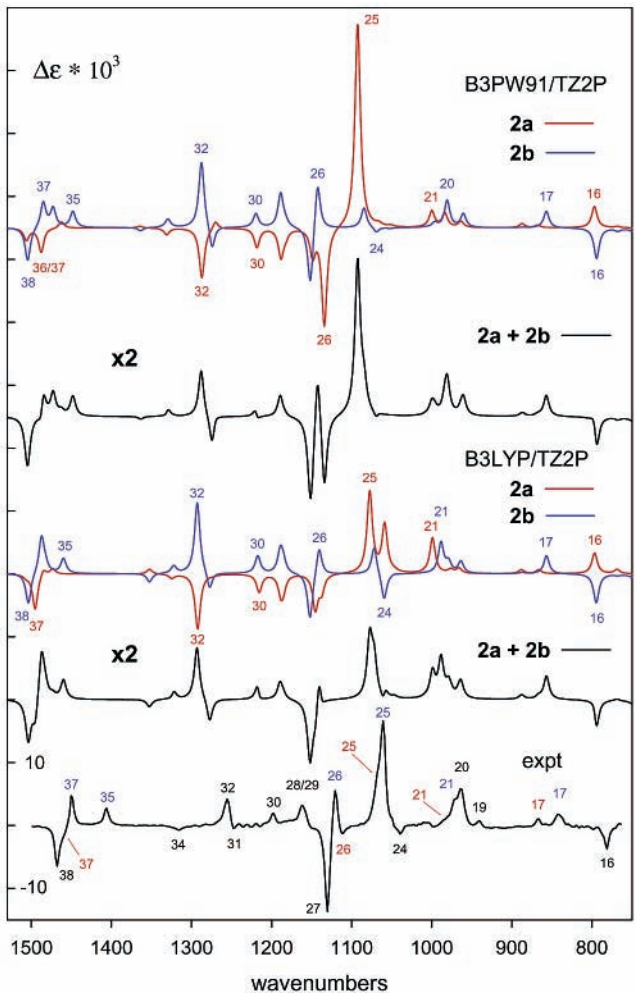

Figure 11. Calculated and experimental VCD spectra of **2**. Calculated spectra are for S-**2**. Spectra of the conformational mixture of **2a** and **2b** are obtained using populations of **2a** and **2b** from Table 2. The experimental spectrum is for (+)-**2** and is from Figure 12. In the assignment of the experimental spectrum, red and blue numbers indicate fundamentals of **2a** and **2b**, respectively; black numbers indicate fundamentals of **2a** and **2b** combined.

ences assuming Boltzmann statistics (Table 2). We have ignored conformation **3d** in Table 7 and Figures 14−16. The predicted percentage population of **3d** is very small (Table 2). Conformationally averaged IR and VCD spectra predicted including **3d** are essentially indistinguishable from those shown in Figures 14−16.

IR and VCD spectra of CCl_4 and CS_2 solutions of **3** have been measured in the mid-IR spectral region. Spectra of **3** in CCl_4 and CS_2 solutions are very similar. Composite IR and VCD spectra are shown in Figure 17. The experimental IR spectrum of **3** is compared to the calculated IR spectra in Figures 14 and 15. Overall, the B3LYP/TZ2P and B3PW91/TZ2P spectra are both in good agreement with the experimental spectrum and permit convincing assignment of the majority of the bands observed experimentally. Our assignment is detailed in Table 7 and Figures 14 and 15. The analysis of the IR spectrum of **3** unambiguously demonstrates the presence of the three conformations, **3a**, **3b**, and **3c**, in CCl_4 and CS_2 solutions. Fundamentals 9−11, 14, 16, 19, 36, and 41 of **3a**, fundamentals 8, 9, 15, and 45 of **3b**, and fundamentals 12, 14, 16, 19, and 30 of **3c** are clearly resolved and unambiguously assignable. Lorentzian fitting of the experimental IR spectrum of **3** leads to the frequencies and dipole strengths given in Table 7. Calculated and experimental frequencies and dipole strengths are compared in Figures 6 and 7. Calculated dipole strengths are conformationally averaged. The agreement is comparable to that observed for **1** and **2**. In the case of the dipole strengths, agreement is good for both functionals, with the exception of modes 26−29.

The experimental VCD spectrum of (+)-**3** is compared to the calculated VCD spectra for S-**3** in Figure 16. VCD originating in fundamentals 19 and 41 of **3a**, fundamentals 19, 28, and 45 of **3b**, and fundamentals 19 and 30 of **3c** is clearly resolved, further substantiating the presence of all three conformations, **3a**, **3b**, and **3c**. In addition, VCD originating in the unresolved fundamentals 18, 28, and 45 of **3a** and **3c**, 36 and 41 of **3b** and **3c**, 30 of **3a** and **3b**, and 20−23, 25−27, 29, 31−35, 37, 38, and 42−44 of **3a**, **3b**, and **3c** is observed. Experimental rotational strengths obtained via Lorentzian fitting of the VCD spectrum are given in Table 7. Calculated and experimental rotational strengths are compared in Figure 8. Calculated rotational strengths are conformationally averaged. Agreement is comparable to that observed for **1** and **2** and is good for both functionals, with the exception of mode 43.

The differences in B3LYP/TZ2P and B3PW91/TZ2P IR and VCD spectra are most pronounced for modes 26−29. B3LYP gives clearly superior agreement with experiment for the dipole strengths of these modes.

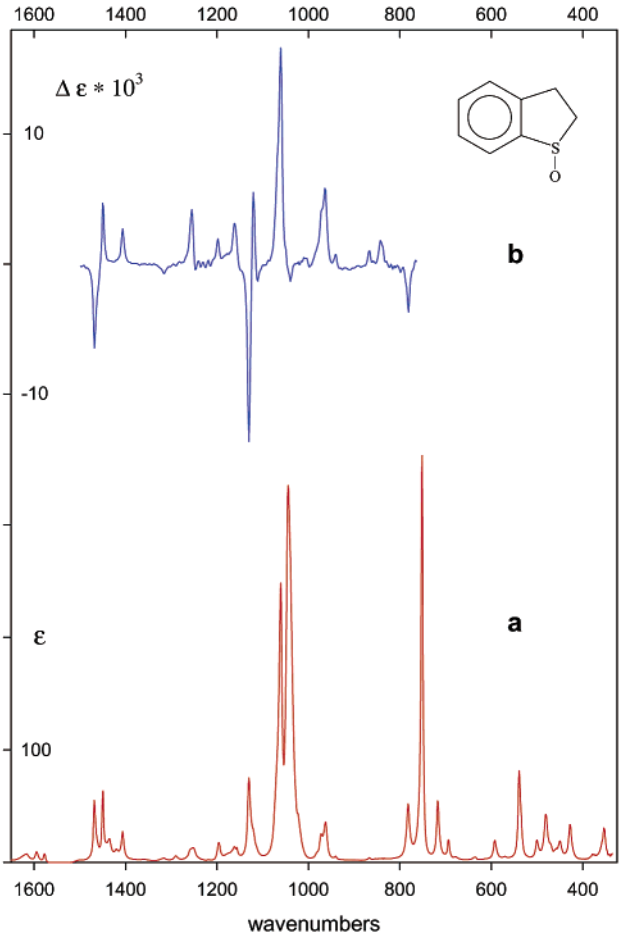

Figure 12. Experimental IR (a) and VCD (b) spectra of **2**: (a) 325−700, 835−1030, and 1090−1650 cm^{-1}, 0.26 M in CCl_4, 597 μ path; 700−835 cm^{-1}, 0.25 M in CS_2, 239 μ path; 1030−1090 cm^{-1}, 0.26 M in CCl_4, 109 μ path; (b) 765−850 and 1070−1095 cm^{-1}, 0.24 M in CS_2, 239 μ path; 850−1025 and 1100−1500 cm^{-1}, 0.26 M in CCl_4, 597 μ path; 1025−1070 cm^{-1}, 0.24 M in CS_2, 109 μ path. The IR spectrum is for (−)-**2**; the VCD spectrum is the "half-difference" spectrum, $(^1/_2)[\Delta\epsilon(+) - \Delta\epsilon(-)]$ (see text).

Discussion

The bicyclic molecules **1**, **2**, and **3** all contain a flexible ring fused to a phenyl ring. The latter constrains the conformations of the former. In **1** and **3**, C3 and S form an essentially planar moiety with the phenyl ring: C3C4C5C6C7C8C9S. In **2**, the planar moiety is C2C3C4C5C6C7C8S. Ring puckering is thus limited to C1 and C2 in **1** and **3** and C1 in **2**. The stable conformations of **1**−**3** have been established by scanning their PESs at the B3LYP/6-31G* level. In **1** and **3**, the scans involve the two dihedral angles C5C4C3C2 and C8C9SC1. In **2**, the PES is scanned with respect to C7C8SC1. In **1** and **2**, two stable conformations are identified; in **3**, there are four. Energy minimization at the B3LYP/6-31G*, B3PW91/6-31G*, B3LYP/TZ2P, and B3PW91/TZ2P levels leads to equilibrium structures for these conformations. The structures of each conformation are qualitatively identical at all four theoretical levels. Quantitatively, the structures are very similar. In particular, in all cases, variations in dihedral angles defining the conformations of the flexible rings are <4°. We have not calculated full PESs at the B3PW91/6-31G*, B3LYP/TZ2P, and B3PW91/TZ2P levels. The variation in the optimized geometries of each conformation on changing the functional to B3PW91 and/or the basis set to TZ2P support the expectation that the PESs are qualitatively identical.

In **1**, **1a** is uniformly lower in energy than **1b** at all four calculational levels. The energy differences, ΔE_{ba}, are <0.9 kcal/mol. In **2**, **2a** is lower than **2b** at the B3LYP/6-31G* and B3PW91/6-31G* levels, but the order is reversed by TZ2P calculations. The energy differences, ΔE_{ba}, are <0.4 kcal/mol in magnitude. In **3**, conformation **3a** is lowest in energy at B3LYP/6-31G*, B3LYP/TZ2P, and B3PW91/TZ2P levels, but at the B3PW91/6-31G* level, **3b** is lower than **3a**. The overall range in energy of **3a**−**3d** is 1.3−1.5 kcal/mol. Conformation **3d** is uniformly significantly higher in energy than **3a**−**3c**. If **3d** is not included, the overall range in energy of **3a**−**3c** is <0.7 kcal/mol. Our DFT calculations lead to the expectation that conformations **1a** and **1b** of **1** and **2a** and **2b** of **2** are sufficiently close in energy that both conformations of both **1** and **2** will be significantly populated at room temperature. In the case of **3**, DFT calculations lead to the expectation that **3a**−**3c** will be significantly populated at room temperature but not **3d**. Predicted conformational energy differences and populations are quite sensitive to the choice of functional and basis set. It is to be expected that the TZ2P basis set results are more accurate than the 6-31G* results. We recognize, however, that *solution* conformational *free energy* differences and populations reflect not only equilibrium geometry energy differences but also zero-point energy, entropy, and solvent effects.

The predicted conformational structures of **1**−**3** can be understood by reference to the structures of the corresponding sulfides. Removal of the sulfoxide O atoms from **1a** and **1b** followed by energy minimization leads to enantiomeric structures of the sulfide, **4**. Key dihedral angles of these two structures, **4a** and **4b**, calculated at the B3LYP/TZ2P level are given in Table 1. The change in geometry of the C1C2C3C4C9S ring is not great. Thus, **1a** and **1b** of the same absolute configuration are essentially diastereoisomeric, combining a stereogenic sulfoxide moiety of the same absolute configuration with enantiomeric C1C2C3C4C9S ring structures. The two conformations **1a** and **1b** are inequivalent and therefore differ in energy. Likewise, conformations **2a** and **2b** can be related to enantiomeric forms of sulfide **5**, **5a** and **5b**. Key dihedral angles of **5a** and **5b** at the B3LYP/TZ2P level are given in Table 4. Again, the changes in geometry from **2a** to **5a** and from **2b** to **5b** are not large. **2a** and **2b** can be regarded as diastereomeric combinations of sulfoxide and enantiomeric C1C2C3C8S ring structures. In the case of **3**, the situation is somewhat more complex. Removal of the sulfoxide O atoms from **3a**−**3d**, followed by optimization, leads to two pairs of enantiomeric structures of the sulfide **6**. In one pair, obtained from **3a** and **3c**, the C1C2C3C4C9S ring is in a chair conformation. In the other pair, obtained from **3b** and **3d**, this ring is in a boat conformation. Key dihedral angles of **6a**−**6d**, at the B3LYP/TZ2P level are given in Table 6. The changes in geometry of the C1C2C3C4C9S ring are small. Thus, **3a** and **3c** of the same absolute configuration are essentially diastereoisomeric combinations of a stereogenic sulfoxide moiety of the same absolute configuration with enantiomeric C1C2C3C4C9S ring structures, as are **3b** and **3d**.

Experimental evidence for the conformations of **1**−**3** predicted by our DFT calculations is provided by their vibrational spectra. We have measured the IR and VCD spectra of CCl_4 and CS_2 solutions of **1**−**3** in the mid-IR spectral region. CCl_4 and CS_2 spectra are very similar, indicating the absence of specific solute−solvent interactions in either solvent. Despite the fairly high (0.05−0.30 M) concentrations used for spectral measurements, in all three molecules IR spectra are unaffected by dilution. Thus, intermolecular aggregation, such as dimer-

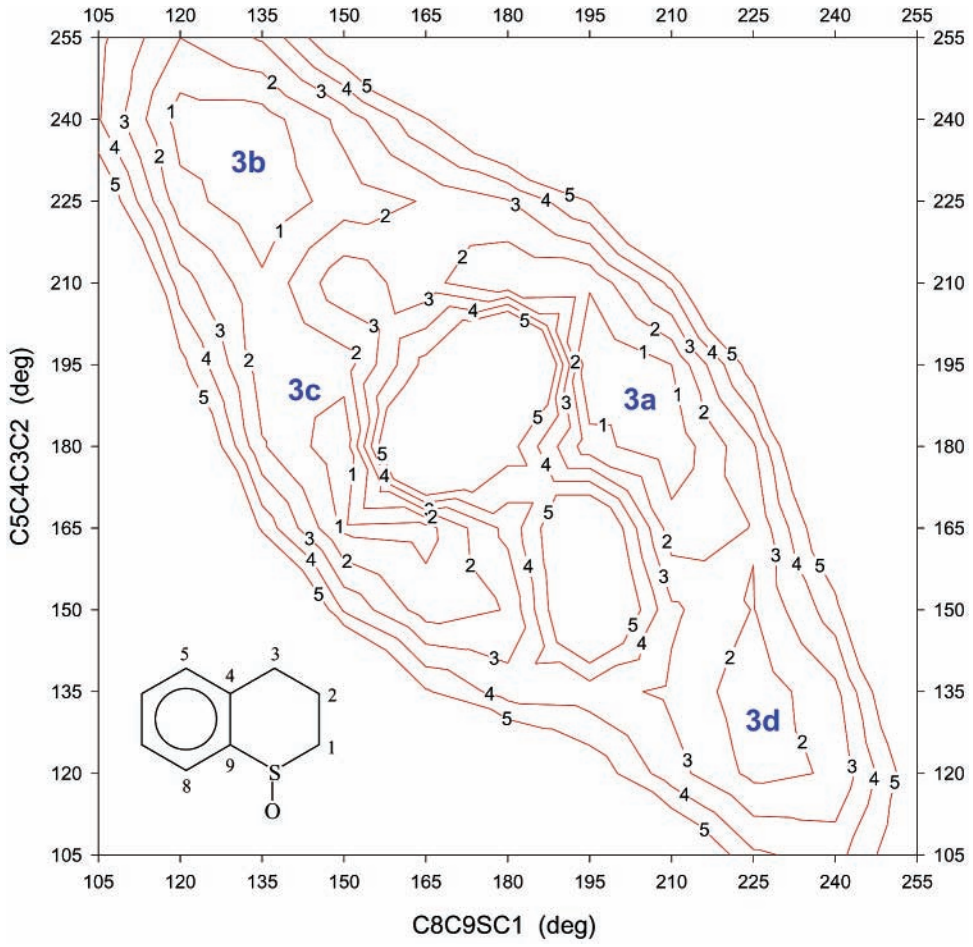

Figure 13. The B3LYP/6-31G* PES of S-**3**. The dihedral angles C5C4C3C2 and C8C9SC1 were varied in 15° steps. Contours are shown at 1 kcal/mol intervals.

TABLE 6: Dihedral Angles of Conformations 3a, 3b, 3c, and 3d[a]

	3a				**3b**			
	6-31G*		TZ2P		6-31G*		TZ2P	
	B3LYP	B3PW91	B3LYP[b]	B3PW91	B3LYP	B3PW91	B3LYP[c]	B3PW91
SC1C2C3	72.9	73.6	72.0 (63.8)	72.8	−19.1	−19.8	−20.3 (−18.7)	−20.8
C1C2C3C4	−48.6	−48.2	−50.6 (−59.3)	−50.0	−40.6	−40.3	−39.4 (−38.4)	−39.3
C2C3C4C9	13.8	12.8	15.8 (27.1)	14.7	52.7	52.7	52.6 (53.9)	52.6
C3C4C9S	−5.7	−4.9	−4.6 (−2.3)	−4.2	1.5	1.5	1.0 (−4.3)	1.1
C4C9SC1	24.2	24.3	20.9 (6.2)	21.6	−51.3	−51.8	−50.9 (−44.4)	−51.5
C9SC1C2	−54.9	−55.6	−51.9 (−35.7)	−53.0	58.4	59.3	59.0 (55.1)	59.8
C5C4C3C2	−168.8	−169.6	−166.0 (−153.5)	−167.0	−126.2	−126.3	−126.5 (−128.9)	−126.6
C8C9SC1	−159.2	−158.7	−161.8 (−175.3)	−160.9	129.3	129.0	129.2 (135.6)	128.9
C8C9SO	91.5	91.9	89.0	89.8	19.0	18.6	19.6	19.1
	3c				**3d**			
	6-31G*		TZ2P		6-31G*		TZ2P	
	B3LYP	B3PW91	B3LYP[d]	B3PW91	B3LYP	B3PW91	B3LYP[e]	B3PW91
SC1C2C3	−72.8	−73.4	−72.8 (−63.8)	−73.4	24.8	26.0	23.7 (18.4)	25.9
C1C2C3C4	45.3	44.6	46.0 (59.4)	45.1	34.9	34.3	34.6 (38.7)	33.2
C2C3C4C9	−11.1	−9.9	−11.5 (−27.2)	−10.1	−51.4	−51.5	−50.3 (−54.0)	−50.3
C3C4C9S	7.9	7.6	7.0 (2.3)	6.8	1.4	1.6	1.2 (4.2)	1.6
C4C9SC1	−29.3	−30.2	−27.8 (−6.1)	−29.0	48.4	48.7	47.5 (44.4)	47.9
C9SC1C2	58.1	59.2	57.2 (35.6)	58.6	−60.1	−61.1	−58.5 (−54.9)	−60.2
C5C4C3C2	172.5	173.6	172.0 (153.4)	173.3	129.4	129.4	130.7 (128.8)	−130.9
C8C9SC1	153.6	152.6	154.8 (175.4)	153.5	−131.6	−131.2	132.6 (−135.6)	−132.0
C8C9SO	40.3	39.0	42.5	40.8	119.0	119.3	118.2	118.8

[a] Dihedral angles in deg for the conformations of S-**3**. See text for atom numbering. [b] Dihedrals in parentheses are for structure **6a**. [c] Dihedrals in parentheses are for structure **6b**. [d] Dihedrals in parentheses are for structure **6c**. [e] Dihedrals in parentheses are for structure **6d**.

ization, which is precedented in sulfoxides,[18] appears to be insignificant for **1**−**3** at the concentrations employed. Analysis of the IR and VCD spectra of **1**−**3** is effected using harmonic spectra predicted at the B3LYP/TZ2P and B3PW91/TZ2P levels.

TABLE 7: Calculated and Experimental Frequencies, Dipole Strengths, and Rotational Strengths for 3[a]

				calculation[c]															
				B3LYP									B3PW91						
	experiment[b]			**a**			**b**			**c**			**a**			**b**			**c**	
mode	ν	D	R	ν	D	R	ν	D	R	ν	D	R	ν	D	R	ν	D	R	ν	D	R
47abc	1595	4.4		1635	4.4	−2.8	1634	1.2	−2.1	1634	1.8	−0.7	1648	5.5	−2.9	1647	1.6	−1.9	1647	2.4	−0.8
46abc	1570	2.4		1608	5.1	0.0	1613	0.4	−0.5	1608	2.2	0.8	1620	6.0	−0.2	1626	0.5	−0.6	1621	2.6	1.0
45ac	1478	29.2	−5.4	1515	30.0	−5.9				1513	39.0	−3.8	1515	33.7	−7.6				1514	44.9	−4.4
45b	1470	15.4	−2.6				1510	14.2	−5.1							1506	39.7	−2.1			
44abc	1449	21.7	−6.3	1498	21.7	0.9	1503	20.6	3.9	1500	22.6	−7.2	1487	26.6	1.4	1497	3.9	3.1	1490	26.6	−8.4
43abc	1442 1437	17.6 20.5	8.0	1480	34.2	−25.7	1494	34.9	−10.8	1485	26.4	16.8	1475	21.9	−4.8	1485	38.7	−30.6	1475	36.6	42.9
42abc	1431	22.3	−8.1	1476	14.3	8.8	1483	16.0	2.7	1477	29.0	−14.1	1469	27.5	−13.2	1478	9.4	26.5	1474	13.7	−28.6
41bc	1422	6.9	1.3				1477	7.1	12.4	1472	7.2	15.1				1465	10.1	7.6	1461	15.0	5.8
41a	1406	17.4	5.2	1459	18.1	5.7							1447	21.4	7.9						
40abc	1348	5.9	−1.6	1388	0.3	1.9	1385	1.3	0.3	1386	0.6	−1.9	1384	0.4	−1.0	1379	1.5	1.4	1382	0.9	8.0
39ac				1385	0.8	−1.9				1384	1.5	8.3	1379	0.4	1.7				1379	0.8	−3.2
39b	1317	4.5					1346	5.9	−18.4							1356	3.9	−9.0			
38abc	1298	9.7	2.8	1328	1.7	1.0	1337	3.9	−2.4	1324	0.4	0.0	1348	1.9	3.0	1339	1.8	−7.6	1346	0.1	0.2
37abc	1283	14.2	−3.2	1321	5.3	0.3	1311	10.2	−9.8	1314	9.4	1.1	1317	6.2	−3.7	1306	12.7	−15.5	1310	11.1	4.3
36a	1259	14.0		1289	24.1	4.8							1283	18.4	4.9						
36bc	1252	4.5	−6.9				1281	3.0	−17.5	1284	20.9	−23.2				1275	2.7	−17.2	1278	17.2	−25.4
35abc	1240	5.9	−5.4	1275	0.4	−1.8	1264	11.7	−10.9	1273	1.1	−1.9	1272	1.2	−3.2	1260	16.5	−15.9	1270	1.6	−2.6
34abc	1195	11.7	4.5	1214	5.2	6.1	1222	3.6	3.2	1213	4.4	0.0	1221	5.8	7.7	1227	3.8	3.0	1219	4.8	−0.6
33abc	1171	20.1	6.0	1196	11.1	10.4	1191	9.4	−5.6	1194	9.7	−7.2	1195	16.2	12.7	1187	14.9	−4.2	1192	23.0	−12.1
32abc	1159	10.4	0.8	1190	4.3	0.7	1186	1.1	−0.1	1188	11.4	−3.2	1186	1.9	0.2	1181	0.6	−0.8	1185	7.1	−0.7
31abc	1131	20.6	7.8	1153	8.7	13.4	1158	2.6	−0.2	1147	1.9	−1.5	1151	20.3	12.2	1154	2.1	−4.0	1150	2.2	−1.2
30ab	1124	11.1	2.0	1145	8.0	1.4	1143	5.1	−2.4				1145	4.5	6.4	1145	5.1	−1.6			
30c	1113	3.2	−5.1							1139	2.6	−7.0							1134	10.4	−12.6
29abc	1077	150.8	6.8	1085	48.1	−1.0	1085	227.5	0.1	1085	153.2	20.8	1090	171.9	−1.9	1102	398.6	8.6	1099	381.4	43.2
28ac	1054	154.8	−23.8	1069	141.5	−31.6				1070	147.5	0.0	1082	259.4	−29.0				1081	42.4	−7.8
28b	1044	281.7	14.3				1059	182.0	−8.7							1071	61.0	−1.0			
27abc				1056	183.4	10.9	1055	84.7	7.9	1061	85.0	−6.4	1068	35.6	10.2	1063	53.5	1.9	1065	50.3	−2.3
26abc				1052	51.8	−0.8	1047	7.3	5.6	1054	94.9	3.7	1059	4.1	−1.0	1055	16.4	4.0	1062	21.5	1.5
25abc	1007	96.6	23.0	1021	79.5	12.8	1029	69.6	19.1	1022	72.2	24.6	1024	30.7	5.2	1025	38.6	14.9	1023	41.0	18.1
24abc				1009	0.9	0.5	1010	1.1	−0.8	1009	1.5	−0.3	1008	0.3	0.2	1008	0.8	−0.7	1008	1.0	−0.4
23abc	948	6.6	−1.0	975	4.4	0.9	976	6.9	−2.3	978	4.0	−0.7	974	3.8	0.7	975	7.5	−2.3	977	4.4	−1.4
22abc	929	34.5	−19.2	941	44.8	−39.0	943	14.4	8.7	942	19.4	25.9	941	39.6	−33.6	942	12.8	8.1	940	15.8	21.5
21abc	886	13.2	1.3	900	16.5	5.4	895	0.7	1.9	899	4.5	4.1	903	20.6	−3.4	895	0.8	1.8	902	9.1	10.8
20abc	865	6.4	7.7	881	6.6	−2.7	875	3.6	2.6	881	15.9	10.8	882	7.0	−1.5	882	4.4	2.1	883	15.4	10.6
19c	845[e]		2.3							862	13.8	5.1							857	16.0	6.6
19a	832[d]	20.6[d]	2.2	849	21.6	1.6							843	26.5	1.4						
19b	810[e]		0.9				821	4.4	10.9							821	4.3	10.7			
18ac	780[d]	29.6[d]	11.4	790	31.7	20.8				788	36.8	−17.4	792	33.0	22.6				790	30.8	−17.2
18b	755[d]	46.1[d]					772	198.8	−25.2							771	224.3	−16.7			
17abc	751[d]	297.8[d]		769	241.8	−1.4	768	110.1	33.6	766	235.1	5.9	768	237.6	−1.3	766	76.2	29.0	766	242.8	1.8
16b							750	25.3	−4.2							749	40.2	−6.8			
16a	711	40.5		731	38.7	0.2							729	42.3	1.1						
16c	706	18.5								726	32.7	−8.6							725	33.9	−8.3
15b	692	16.3					699	72.3	−7.0							710	73.8	−5.2			
14b							690	0.8	1.5							691	2.1	3.0			
15ac	675	20.1		680	11.1	−0.8				684	20.8	−4.0	681	16.3	−0.2				690	47.7	−9.5
14c	662	7.9								656	70.7	−8.9							665	47.2	−4.6
14a	648	35.2		625	65.4	2.1							640	73.7	7.6						
13b	590	5.5					598	8.9	7.3							598	8.6	7.1			
13ac	582	23.1		587	48.4	27.3				593	5.8	0.2	588	35.2	24.6				591	5.7	−0.7
12ab	540	74.0		543	75.9	−21.0	545	33.1	−16.0				544	81.0	−21.1	544	32.2	−15.8			
12c	529	39.2								536	58.1	−2.9							535	55.8	−3.0
11a	494	23.6		501	18.6	1.8							500	16.1	1.6						
11bc	484	2.8					483	27.5	−0.8	487	22.6	2.5				485	27.4	−1.0	489	20.0	2.5
10a	461	74.5		468	65.9	−0.1							466	66.0	−1.4						
10bc	450	42.1					451	69.4	6.5	459	67.2	−14.3				450	68.9	6.3	457	71.7	−14.5
9a	438	60.2		435	60.8	21.1							438	68.5	23.5						
9b	423	16.2					425	54.8	1.5							427	47.7	1.3			
8a/9c	398	113.0		397	145.7	−17.1				396	88.5	−2.2	397	126.3	−19.3				398	76.4	−2.4
8bc	370	19.8					378	17.4	−1.0	367	6.3	−2.6				379	14.2	−0.3	369	9.7	−0.1
7				333	16.1	−7.5	347	41.8	6.6	346	43.3	1.3	331	15.9	−8.2	345	39.4	6.5	348	35.4	0.7
6				303	7.3	−4.0	333	51.0	0.5	338	42.9	15.9	302	9.3	−6.2	333	53.2	−0.1	336	45.8	15.4

[a] Frequencies, ν, in cm^{-1}; dipole strengths, D, in 10^{-40} esu^2 cm^2; rotational strengths, R, in 10^{-44} esu^2 cm^2. Experimental rotational strengths are for (+)-**3**; calculated rotational strengths are for S-**3**. [b] From Lorentzian fitting of IR spectrum in CCl_4 solution, unless indicated. [c] TZ2P basis set. [d] CS_2 solution IR spectra. [e] CS_2 solution VCD spectra.

For each molecule, spectra are conformationally averaged. Spectra calculated for each conformation are summed, with conformational populations obtained from calculated energy differences using Boltzmann statistics. As is clearly shown in Figures 3, 4, 10, 11, and 14−16, both IR and VCD spectra are highly conformation-dependent. As a result, conformationally averaged spectra are substantially different from the spectra of individual conformations. Many more transitions are predicted

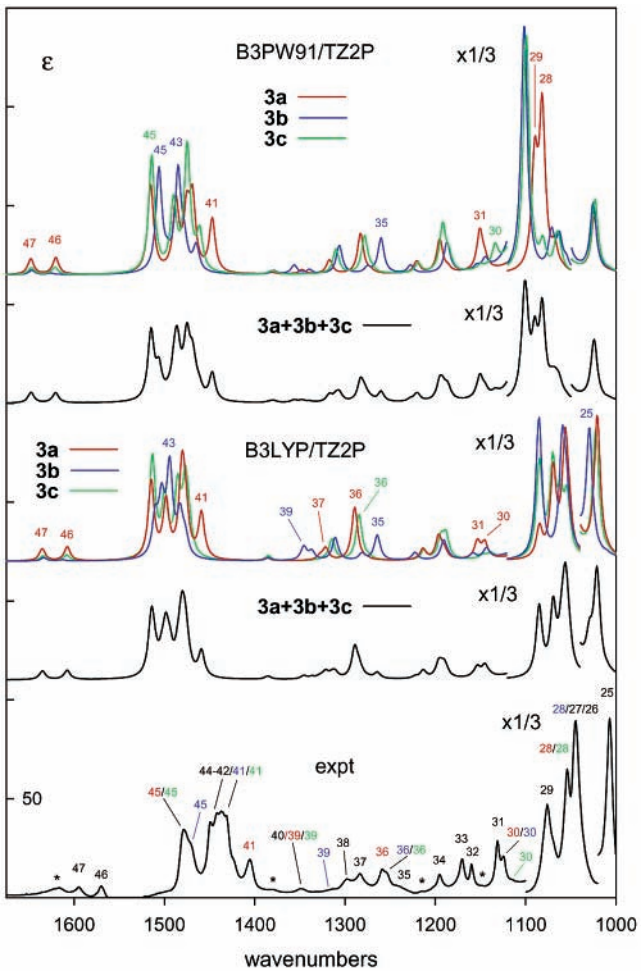

Figure 14. Calculated and experimental IR spectra of **3** at $\nu > 1000$ cm^{-1}. Spectra of the conformational mixture of **3a**, **3b**, and **3c** are obtained using populations of **3a**, **3b**, and **3c** from Table 2. The experimental spectrum is from Figure 17. In the assignment of the experimental spectrum, red, blue, and green numbers indicate fundamentals of **3a**, **3b**, and **3c**, respectively, while black numbers indicate fundamentals of **3a**, **3b**, and **3c** combined. Asterisks indicate bands not assigned to fundamentals of **3**.

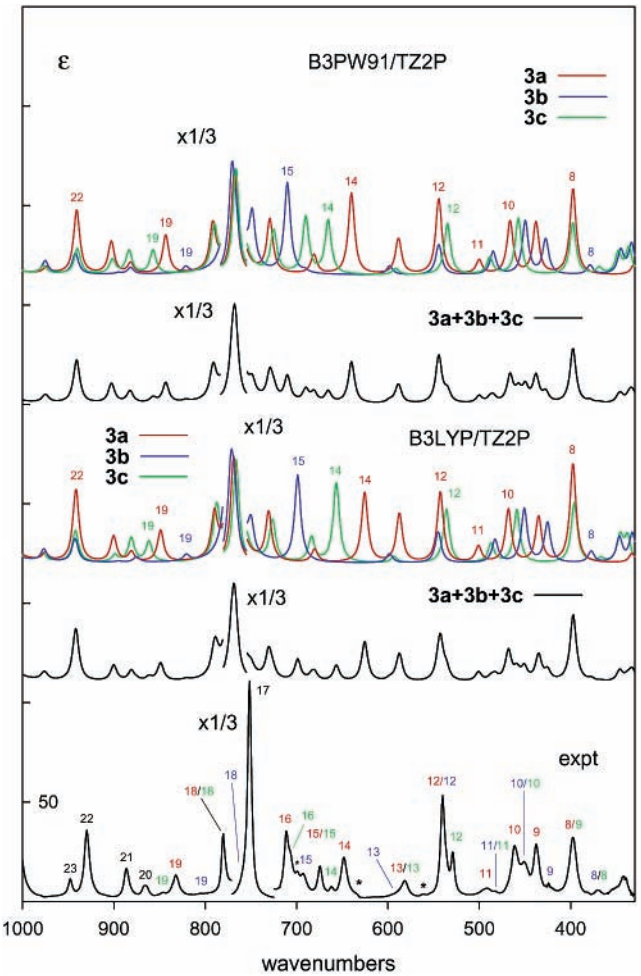

Figure 15. Calculated and experimental IR spectra of **3** at $\nu < 1000$ cm^{-1}. Spectra of the conformational mixture of **3a**, **3b**, and **3c** are obtained using populations of **3a**, **3b**, and **3c** from Table 2. The experimental spectrum is from Figure 17. In the assignment of the experimental spectrum, red, blue, and green numbers indicate fundamentals of **3a**, **3b**, and **3c**, respectively, while black numbers indicate fundamentals of **3a**, **3b**, and **3c** combined. Asterisks indicate bands not assigned to fundamentals of **3**.

than for a single conformation, i.e., conformational splittings are observed. Even when conformational splittings are small, intensity patterns are different. The predicted IR and VCD spectra for **1**−**3** are in good overall agreement with the corresponding experimental spectra. In each molecule, the experimental IR spectrum over the range 300−1700 cm^{-1} exhibits a substantially larger number of transitions than the number of fundamentals expected for a single conformation. In each case, all but an extremely small number of experimental bands can be assigned to predicted transitions. (Bands not assigned to fundamentals are assigned either to overtone/combination bands or to impurities.) The experimental IR spectra thus unambiguously confirm the presence of the predicted conformations. The experimental VCD spectra further support the analysis of the IR spectra. Despite the smaller accessible frequency range (>700 cm^{-1}) and the poorer signal-to-noise ratios of the VCD spectra, it is again the case that in each molecule more bands are observed than can be accounted for by a single conformation and that in each case very nearly all observed bands can be assigned to predicted transitions.

We have predicted IR and VCD spectra using two different functionals, B3LYP and B3PW91. Overall, predicted spectra are insensitive to the choice of functional. However, in some spectral regions, considerably greater sensitivity is found. The most dramatic variations occur in the vicinity of the S−O stretching mode. In **1a** and **1b**, the IR and VCD of modes 27−32 vary dramatically with functional. In **2a** and **2b**, modes 23−27 are similarly functional-dependent. Analogous sensitivity occurs in **3a**, **3b**, and **3c** for modes 26−29. Assignments are most certain when the two functionals give qualitatively identical predictions of both IR and VCD spectra and when the predicted IR and VCD spectra are in qualitative agreement with the experimental spectra. When predicted spectra vary substantially with functional, assignments are less certain. It is important to point out that for the large majority of the IR and VCD spectra of **1**−**3**, B3LYP and B3PW91 spectra are both qualitatively identical and in qualitative agreement with experimental spectra. Thus, even if spectral regions where assignments are less certain are excluded, the conformational analysis remains secure.

Our assignments of the IR and VCD spectra of **1**−**3** are further supported by quantitative comparisons of calculated and experimental frequencies, dipole strengths, and rotational strengths. Experimental parameters are obtained by Lorentzian fitting. Comparisons of frequencies are shown in Figure 6. Calculated frequencies are, with relatively few exceptions, greater than

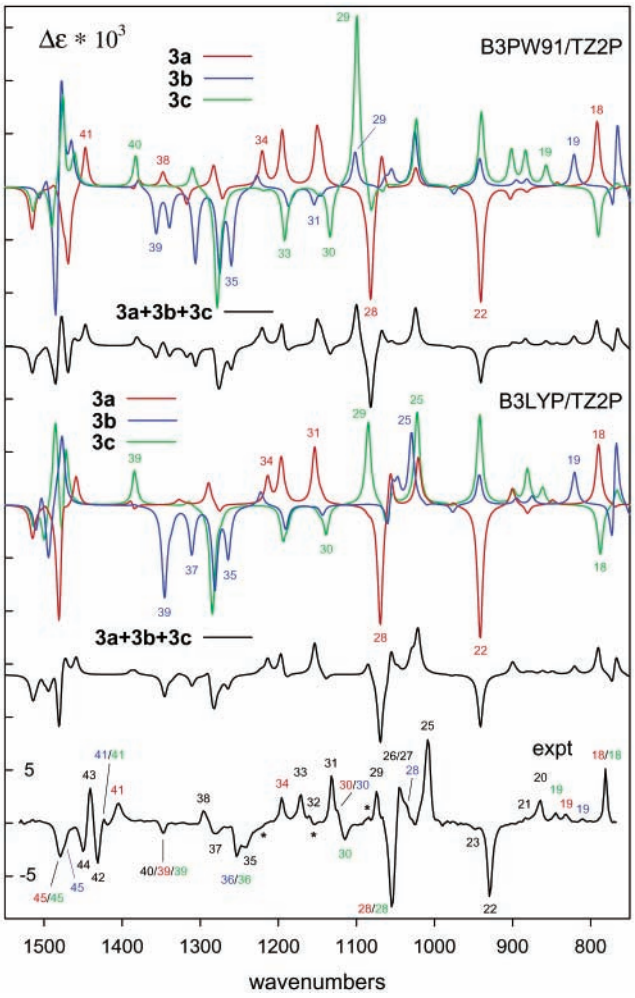

Figure 16. Calculated and experimental VCD spectra of **3**. Calculated spectra are for S-**3**. Spectra of the conformational mixture of **3a**, **3b**, and **3c** are obtained using populations of **3a**, **3b**, and **3c** from Table 2. The experimental spectrum is for (+)-**3** and is from Figure 17. In the assignment of the experimental spectrum, red, blue, and green numbers indicate fundamentals of **3a**, **3b**, and **3c**, respectively; black numbers indicate fundamentals of **3a**, **3b**, and **3c** combined.

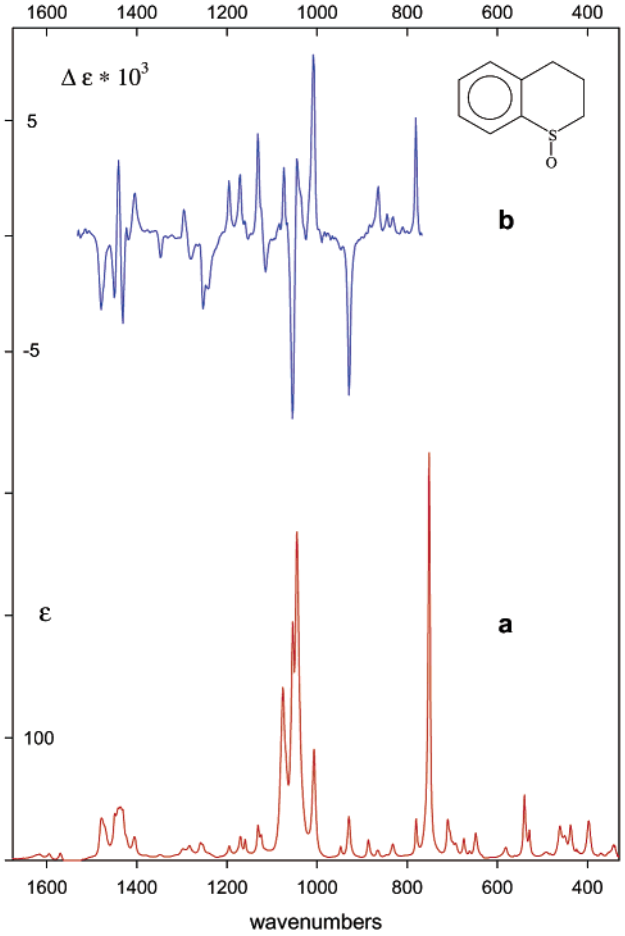

Figure 17. Experimental IR (a) and VCD (b) spectra of **3**: (a) 330−720, 835−1015, and 1065−1675 cm^{-1}, 0.30 M in CCl_4, 597 μ path; 700−835 cm^{-1}, 0.29 M in CS_2, 109 μ path; 1015−1065 cm^{-1}, 0.30 M in CCl_4, 109 μ path; (b) 765−845 cm^{-1}, 0.29 M in CS_2, 597 μ path; 845−985 and 1085−1530 cm^{-1}, 0.30 M in CCl_4, 597 μ path; 985−1035 cm^{-1}, 0.30 M in CCl_4, 239 μ path; 1035−1085 cm^{-1}, 0.30 M in CCl_4, 109 μ path. The IR spectrum is for (+)-**3**; the VCD spectrum is the "half-difference" spectrum, $(^1/_2)[\Delta\epsilon(+) - \Delta\epsilon(-)]$ (see text).

experimental frequencies, the differences lying in the range 0−5% and generally increasing with increasing vibrational frequency. The quantitative agreement of calculated and experimental frequencies is typical of B3LYP and B3PW91 frequencies calculated at the TZ2P basis set level.[12,17] A large fraction of the deviations can be attributed to anharmonicity,[19] which is not included in the calculated frequencies. Comparisons of dipole strengths and rotational strengths are shown in Figures 7 and 8, respectively. Again, the level of agreement is typical.[12,17] Note that the modes whose dipole strengths and/or rotational strengths are in the poorest agreement with experiment also exhibit large variations with functional.

The quantitative agreement of calculated and experimental frequencies, dipole strengths, and rotational strengths for **1**−**3** leads to the conclusions that (1) the IR and VCD spectra of the individual conformations of **1**−**3** are predicted with a reliability typical of harmonic B3LYP/TZ2P and B3PW91/TZ2P calculations and (2) the populations of the individual conformations of **1**−**3** used in predicting IR and VCD spectra are of the correct order of magnitude. The former conclusion allows us to further conclude that the geometrical structures of the conformations of **1**−**3** are accurately predicted since vibrational spectra are a sensitive function of equilibrium geometry and, therefore, if the structures were far from correct the associated vibrational spectra would be also. The second conclusion supports our earlier expectation that conformational energies and populations calculated at the TZ2P basis set level should be more accurate than 6-31G* values.

The absolute configuration (AC) of **2** was first assigned as *S*(+)/*R*(−) by Yamagishi et al.[20] by comparison of the optical rotatory dispersion (ORD) of the *N*-*p*-toluenesulfonylimide (NTs) of **2** to the ORD of (*p*-Tol)S(NTs)CH_3, whose AC had previously been determined by X-ray crystallography. The ACs of **1** and **3** were subsequently assigned as *S*(+)/*R*(−) by Allenmark and Andersson[21] and Takata et al.,[22] respectively, by comparison of their UV CD to that of **2**. The agreement of predicted and experimental vibrational rotational strengths exhibited in Figure 8 unambiguously confirms the earlier assignments of the ACs of **1**, **2**, and **3**.

Conclusion

Our analyses of the IR and VCD spectra of **1**, **2**, and **3** have demonstrated unambiguously the presence in CCl_4 and CS_2 solutions of the two conformations of **1**, **1a** and **1b**, the two conformations of **2**, **2a** and **2b**, and the three conformations of **3**, **3a**, **3b**, and **3c**, predicted by DFT (B3LYP and B3PW91) calculations. Out results further demonstrate the utility of IR and VCD spectroscopies, in combination with DFT, in carrying out the conformational analysis of flexible organic molecules.

Acknowledgment. Financial support by NSF (Grant CHE-9902832) to P.J.S. and by Università della Basilicata (Potenza) and MURST (Rome) to C.R., S.S., and P.S. is gratefully acknowledged. Ab initio computations were carried out at the USC Research Computing Facility using SGI Origin 2000 and Pentium III cluster machines.

Supporting Information Available: Methods used to synthesize **1**, **2**, and **3**. This material is available free of charge via the Internet at http://pubs.acs.org.

References and Notes

(1) Stephens, P. J.; Devlin, F. J. *Chirality* **2000**, *12*, 172.

(2) (a) Johnson, B. G.; Frisch, M. J. *Chem. Phys. Lett*. **1993**, *216*, 133. (b) Johnson, B. G.; Frisch, M. J. *J. Chem. Phys*. **1994**, *100*, 7429.

(3) Cheeseman, J. R.; Frisch, M. J.; Devlin, F. J.; Stephens, P. J. *Chem. Phys. Lett*. **1996**, *252*, 211.

(4) (a) London, F. *J. Phys. Radium* **1937**, *8*, 397. (b) Ditchfield, R. *Mol. Phys*. **1974**, *27*, 789.

(5) Becke, A. D. *J. Chem. Phys.* **1993**, *98*, 1372, 5648.

(6) Devlin, F. J.; Stephens, P. J. *J. Am. Chem. Soc*. **1999**, *121*, 7413.

(7) Aamouche, A.; Devlin, F. J.; Stephens, P. J. *J. Am. Chem. Soc*. **2000**, *122*, 7358.

(8) (a) Cheeseman, J. R.; Frisch, M. J.; Devlin, F. J.; Stephens, P. J. *J. Phys. Chem. A* **2000**, *104*, 1039. (b) Stephens, P. J.; Devlin, F. J.; Cheeseman, J. R.; Frisch, M. J. *J. Phys. Chem. A* **2001**, *105*, 5356. (c) Furche, F.; Alrichs, R.; Wachsmann, C.; Weber, E.; Sobanski, A.; Vögtle, F.; Grimme, S. *J. Am. Chem. Soc*. **2000**, *122*, 1717.

(9) Stephens, P. J.; Devlin, F. J.; Cheeseman, J. R.; Frisch, M. J.; Scafato, P.; Superchi, S.; Rosini, C., to be submitted for publication.

(10) (a) Brunel, J.; Diter, P.; Duetsch, M.; Kagan, H. B. *J. Org. Chem*. **1995**, *60*, 8086. (b) Donnoli, M. I.; Superchi, S.; Rosini, C. *J. Org. Chem*. **1998**, *63*, 9392.

(11) Lupatelli, P.; Ruzziconi, R.; Scafato, P.; Degl′Innocenti, A.; Belli Paolobelli, A. *Synth. Commun*. **1997**, *27*, 441.

(12) (a) Devlin, F. J.; Stephens, P. J.; Cheeseman, J. R.; Frisch, M. J. *J. Phys. Chem. A* **1997**, *101*, 6322. (b) Devlin, F. J.; Stephens, P. J.; Cheeseman, J. R.; Frisch, M. J. *J. Phys. Chem. A* **1997**, *101*, 9912.

(13) Frisch, M. J.; Trucks, G. W.; Schlegel, H. B.; Scuseria, G. E.; Robb, M. A.; Cheeseman, J. R.; Zakrzewski, V. G.; Montgomery, J. A., Jr.; Stratmann, R. E.; Burant, J. C.; Dapprich, S.; Millam, J. M.; Daniels, A. D.; Kudin, K. N.; Strain, M. C.; Farkas, O.; Tomasi, J.; Barone, V.; Cossi, M.; Cammi, R.; Mennucci, B.; Pomelli, C.; Adamo, C.; Clifford, S.; Ochterski, J.; Petersson, G. A.; Ayala, P. Y.; Cui, Q.; Morokuma, K.; Malick, D. K.; Rabuck, A. D.; Raghavachari, K.; Foresman, J. B.; Cioslowski, J.; Ortiz, J. V.; Stefanov, B. B.; Liu, G.; Liashenko, A.; Piskorz, P.; Komaromi, I.; Gomperts, R.; Martin, R. L.; Fox, D. J.; Keith, T.; Al-Laham, M. A.; Peng, C. Y.; Nanayakkara, A.; Gonzalez, C.; Challacombe, M.; Gill, P. M. W.; Johnson, B. G.; Chen, W.; Wong, M. W.; Andres, J. L.; Head-Gordon, M.; Replogle, E. S.; Pople, J. A. *Gaussian 98*; Gaussian, Inc.: Pittsburgh, PA, 1998.

(14) Stephens, P. J.; Devlin, F. J.; Chabalowski, C. F.; Frisch, M. J. *J. Phys. Chem*. **1994**, *98*, 11623.

(15) Hehre, W. J.; Schleyer, P. R.; Radom, L.; Pople, J. A. *Ab Initio Molecular Orbital Theory*; Wiley: New York, 1986.

(16) Stephens, P. J.; Jalkanen, K. J.; Amos, R. D.; Lazzeretti, P.; Zanasi, R. *J. Phys. Chem.* **1990**, *94*, 1811.

(17) (a) Stephens, P. J.; Ashvar, C. S.; Devlin, F. J.; Cheeseman, J. R.; Frisch, M. J. *Mol. Phys*. **1996**, *89*, 579. (b) Devlin, F. J.; Stephens, P. J. *J. Phys. Chem. A* **1999**, *103*, 527. (c) Ashvar, C. S.; Devlin F. J.; Stephens, P. J. *J. Am. Chem. Soc*. **1999**, *121*, 2836.

(18) (a) Watson, R. F.; Eastham, J. F. *J. Am. Chem. Soc*. **1965**, *87*, 664. (b) Mislow, K.; Green, M. M.; Laur, P.; Melillo, J. T.; Simmons, T.; Ternay, A. L. *J. Am. Chem. Soc*. 1**965**, *87*, 1958. (c) Mislow, K.; Green, M. M.; Laur, P.; Chisholm, D. R. *J. Am. Chem. Soc*. **1965**, *87*, 665. (d) Figueroa, R. H.; Roig, E.; Szmant, H. H. *Spectrochim. Acta* **1966**, *22*, 587.

(19) Finley, J. W.; Stephens, P. J. *J. Mol. Struct. (THEOCHEM)* **1995**, *357*, 225.

(20) Yamagishi, F. G.; Rayner, D. R.; Zwicker, E. T.; Cram, D. J. *J. Am. Chem. Soc*. **1973**, *95*, 1916.

(21) (a) Allenmark, S. G.; Andersson, M. A. *Tetrahedron: Asymmetry* **1996**, *7*, 1089. (b) Allenmark, S. G.; Andersson, M. A. *Chirality* **1998**, *10*, 246.

(22) Takata, T.; Yamazaki, M.; Fujimori, K.; Kim, Y. H.; Iyanagi, T.; Oae, S. *Bull. Chem. Soc. Jpn.* **1983**, *56*, 2300.